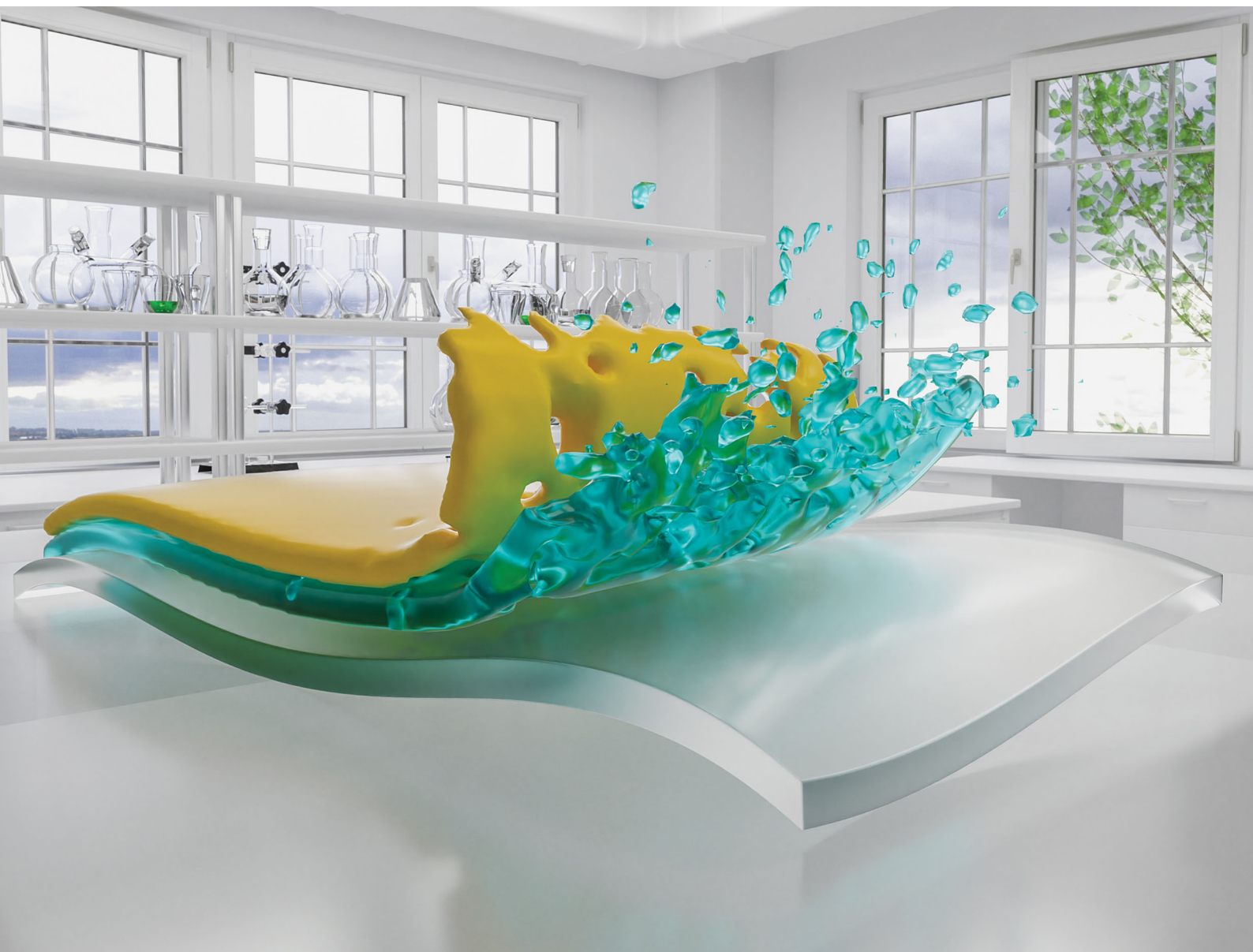


Volume 9  
Number 1  
7 January 2021  
Pages 1–360

# Journal of Materials Chemistry C

Materials for optical, magnetic and electronic devices

[rsc.li/materials-c](http://rsc.li/materials-c)



ISSN 2050-7526



## REVIEW ARTICLE

Marie D. M. Faure and Benoît H. Lessard  
Layer-by-layer fabrication of organic photovoltaic devices:  
material selection and processing conditions

Cite this: *J. Mater. Chem. C*, 2021,  
9, 14

# Layer-by-layer fabrication of organic photovoltaic devices: material selection and processing conditions

Marie D. M. Faure<sup>a</sup> and Benoît H. Lessard \*<sup>ab</sup>

Layer-by-layer (LbL) processing, otherwise known as sequential deposition, is emerging as the most promising strategy for fabrication of active layers in organic photovoltaic (OPV) devices on both laboratory and industrial scales. In comparison to the bulk heterojunction (BHJ) configuration, LbL facilitates separate and sequential deposition of each layer, enabling greater control and optimization of interfaces and final donor/acceptor morphology. Furthermore, this process encourages formation of an efficient vertical phase separation, where the acceptor and donor aggregations are largest at their respective electrodes, increasing exciton dissociation and transport while reducing unwanted charge recombination. Compared to BHJ OPVs, LbL OPVs are more robust, with less dependence on processing conditions, resulting in increased photo, thermal, and mechanical stability and greater power conversion efficiency retention when applied to large area modules. These advantages have resulted in significant interest in the LbL process and its potential to displace BHJ as the dominant process for large-scale OPV manufacturing. This review summarizes recent developments in OPV fabrication through LbL, with particular emphasis on material selection and thin film processing conditions.

Received 31st August 2020,  
Accepted 20th October 2020

DOI: 10.1039/d0tc04146g

rsc.li/materials-c

## 1. Introduction

Organic carbon-based photovoltaics (OPVs) are a viable route towards highly flexible, semi-transparent, low manufacturing cost solar cells with an energy payback time on the order of months.<sup>1,2</sup> While previously disparaged as low performing, over

<sup>a</sup> Department of Chemical and Biological Engineering, University of Ottawa,  
161 Louis Pasteur, Ottawa, Ontario, K1N 6N5, Canada.  
E-mail: benoit.lessard@uottawa.ca

<sup>b</sup> School of Electrical Engineering and Computer Science, University of Ottawa,  
800 King Edward Ave. Ottawa, Ontario, K1N 6N5, Canada



Marie D. M. Faure

Marie D. M. Faure received her master's degree in physics and chemistry from the Graduate School of Chemistry, Biology and Physics of Bordeaux in 2017. She is now a PhD student at the University of Ottawa in the Lessard Research Group. Her research interests are focused on inverted organic solar cells, novel small molecules acceptors for fullerene-free organic solar cells, and processes for bilayer organic solar cell devices fabrication.



Benoît H. Lessard

Benoît Lessard obtained his PhD (2012) from McGill University in Polymer synthesis and reaction engineering. He then completed an NSERC Banting Fellowship at the University of Toronto studying crystal engineering and OPV/OLED fabrication. In 2015, Prof. Benoît H. Lessard joined the Department of Chemical & Biological Engineering at University of Ottawa as an Assistant Professor, and was promoted to Associate Professor in May 2019. Lessard was awarded the Tier 2 Canada Research Chair, 2018 Ontario Early Researcher Award, the 2015 Charles Polanyi Prize in Chemistry and named one of the 2018 *J. Mater. Chem. C* Emerging Researchers. For a full list of publications see: [www.benoitlessard.com](http://www.benoitlessard.com)



the past 5 years OPV cell efficiencies have increased dramatically, now exceeding 18% and evolving into the realm of commercially viable technology.<sup>3</sup> Development of large-scale manufacturing of OPVs necessitates consideration and optimization of several parameters. A crucial design component is choice of materials, as synthetic complexity will dictate if mass production is feasible, with low yields and significant waste streams being prohibitive. Another key aspect is how the active films are fabricated and processed. Bulk production of devices with consistent thin film morphology and performance is critical, requiring large operating windows and the ability to adjust parameters “on-the-fly” with changing environmental conditions such as humidity or temperature.

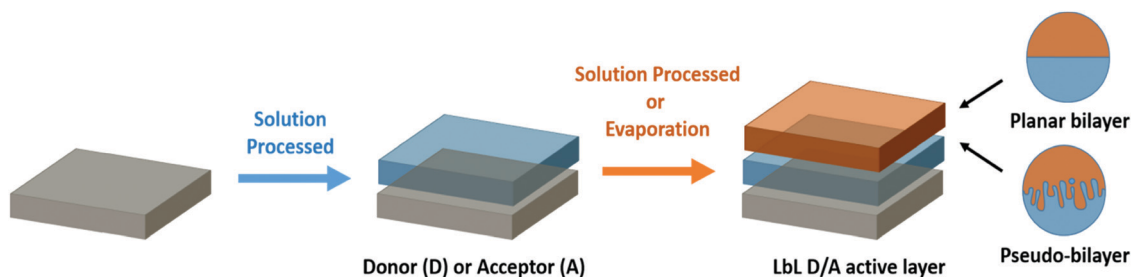
High-performing OPVs have an active layer comprised of at least two different materials, referred to as electron donors and electron acceptors. The prerequisite for multiple materials with complimentary energy levels to provide a driving force to facilitate charge separation of photogenerated excitons is the subject of several excellent reviews.<sup>4–6</sup> Tang and coworkers seminal work was realized by sequentially evaporating thin films of donor and acceptor molecules in a planar heterojunction (PHJ) configuration.<sup>7</sup> Photogenerated excitons can only become free carriers when they reach the donor/acceptor interface, with a typical exciton diffusion length of 5–15 nm, emphasizing the significance of maximizing the interfacial area.<sup>8</sup> The low interfacial area between the donor and acceptor in PHJ bilayer cells severely curtails performances. PHJ OPVs were quickly surpassed by bulk heterojunction (BHJ) devices, which involve blending the materials in a common solvent before deposition, facilitating the forming of a random interpenetrating network with increased donor/acceptor interfacial area.<sup>9</sup> The BHJ architecture has since become widely implemented in research laboratories, affording a facile processing route for the investigation of large families of donor and acceptor materials.<sup>3,6,10–18</sup>

Despite the pervasiveness of the BHJ process, fundamental problems remain in both the fabrication and resulting morphology. The major impediment with BHJ devices is that optimal nanoscale morphology must be spontaneously achieved through a fast deposition and drying. Often the thermodynamically favourable morphology does not yield preminent device performance, requiring optimization of multiple experimental conditions to promote kinetic film formation. Choice of solvents and additives, processing conditions (such as concentration), shearing speed or

drying time, spin speed, ambient conditions such as humidity and temperature, and post annealing steps can all dramatically alter performance.<sup>19</sup> Small changes in processing conditions or operating environment can provoke a transition to another equilibrium state, inducing unfavourable phase separation.<sup>20,21</sup> The blended nature of BHJ devices makes it challenging to predict and understand how changing one variable will affect the overall nanoscale morphology. The optimal intertwined donor/acceptor morphology, comprised of desirable distribution of components, crystallinity, domain sizes, and molecular order and orientation, is very elaborate. This complexity is amplified when transitioning from lab-scale to commercial-scale, illustrating a significant disadvantage with the BHJ process. The ideal OPV manufacturing process would enable deposition of the donor and acceptor independently as two separate layers, allowing intelligent control over each layer, mimicking conventional printing processes while still maximizing interfacial contact.

A pseudo-bilayer configuration *via* layer-by-layer (LbL) fabrication facilitates the combination of facile single-layer deposition processes with improved interfacial contact achieved through BHJ architecture. LbL involves the sequential deposition of the OPV active layers by solution processing for the first layer (often the donor in a direct device configuration) followed by either the evaporation or solution deposition of the second layer (the acceptor in direct device configuration, Scheme 1). Sequential deposition offers a promising route towards commercialization of OPVs through numerous advantages. Each material is deposited independently, allowing control and optimization over discrete layers. Characterization of the interface is facile, which expedites understanding the connection between physical processes and morphology with device performance. The fabrication process results in efficient vertical phase separation, which can be tuned to improve exciton dissociation and reduce charge carrier recombination. Finally, LbL devices have better thermal stability and the technique reduces the dependence on processing conditions, facilitating an easier transition from lab-scale to commercial-scale, with efficiency retention for increased area.

Ayzner *et al.* explored this strategy to address the inherent problems in BHJ fabrication.<sup>22</sup> They deposited poly(3-hexylthiophene) (P3HT) and [6,6]-phenyl-C<sub>61</sub>-butyric acid methyl ester (PC<sub>61</sub>BM) separately from orthogonal solvents and achieved OPV devices nearly as efficient as their blended counterparts. Characterization of interfacial morphology exposed the formation



**Scheme 1** Diagram of pseudo-bilayer or planar bilayer configuration *via* a layer-by-layer (LbL) sequential deposition of the donor and acceptor materials.



of a three-layer structure, with an intermixed donor/acceptor layer sandwiched between two relatively pure donor and acceptor layers.<sup>23</sup> Subsequent studies revealed that sequentially processed devices could be more efficient than BHJ OPVs due to improved vertical phase separation, which enabled stronger photon absorption, higher hole mobility, better charge extraction, and improved thermal stability.<sup>24–26</sup> Optimal vertical grading of the layers can be achieved through controlled swelling of the donor layer, with the magnitude of intermixing with the acceptor modulated by choosing suitable solvents, cosolvents, or solvent additives.<sup>27</sup> The versatility of LbL fabrication was bolstered by the discovery that stringent orthogonal solvents are not required. LbL OPVs have been fabricated using the same solvent for both layers, achieving higher power conversion efficiencies (PCEs) and increased area modules through improved control over morphology and reduced dependence on processing conditions.<sup>28–30</sup> Cells produced through LbL outperformed their BHJ equivalents on both small and very large areas up to 11.52 cm<sup>2</sup>, resulting in the record efficiency reported for a large-area OPV module of 12%.<sup>31</sup>

This review highlights the growth and potential of this fabrication process through exploring studies that focus on LbL processing of OPVs. Particular focus is devoted to the choice and combination of donor and acceptor materials in the active layer, processing conditions, and the translation to large-scale production.

## 2. Material selection for layer-by-layer (LbL) deposition

Since the first report in 2009, a plethora of different donor and acceptor materials have been incorporated into LbL OPVs. While many of these material combinations have also been explored in BHJ OPV configuration, this review will predominantly focus on their performance in LbL OPVs, referencing BHJ performance when used as controls. Candidate donor and acceptor materials for LbL OPVs can be classified as either small molecules or polymers.

### 2.1. Fullerene small molecule acceptors

Since its discovery in 1985, buckminsterfullerene C<sub>60</sub> (Fig. 1, a1) has prompted significant interest in the OPV community due to its efficiency at accepting and transferring electrons, with charge mobilities on the order of 10<sup>-4</sup> to 10<sup>-3</sup> cm<sup>2</sup> V<sup>-1</sup> s<sup>-1</sup>.<sup>32</sup> Haddon *et al.* determined that this proficiency may be due to the curvature of the fullerene surface, which results in a variable intermediate hybridization between sp<sup>2</sup> and sp<sup>3</sup>.<sup>33</sup> Other interesting properties include the functionalization capacity of the surface, along with a photoinduced charge separation acceleration, and a delayed charge recombination in the dark.<sup>34</sup> However, due to its low solubility and high tendency of aggregation, C<sub>60</sub> incorporation into LbL processed OPV devices is always performed *via* thermal evaporation.<sup>35</sup> The use of PC<sub>61</sub>BM (Fig. 1, a2), a soluble C<sub>60</sub> derivative,<sup>36</sup> enabled a significant increase in the availability of dissociation interfaces with the donor by promoting deeper interdiffusion and better carrier collection efficiency. Interdiffusion is also encouraged by π–π interactions between the phenyl groups of PC<sub>61</sub>BM with both itself and with aromatic groups of donor polymers.<sup>37</sup> C<sub>60</sub> and PC<sub>61</sub>BM have wide band gaps of around 2 eV (HOMO = -5.9 eV, LUMO = -3.9 eV) that cover the UV-region, with a weak absorption in the visible region of the solar spectrum. Increasing the fullerene molecular weight from C<sub>60</sub> to C<sub>70</sub> (Fig. 1, a4), or from PC<sub>61</sub>BM to PC<sub>71</sub>BM (Fig. 1, a5), results in a slight red-shift of the absorption into the 400–600 nm range, and a corresponding increase in the short circuit current (*J*<sub>sc</sub>).<sup>38</sup>

Other families of soluble fullerene compounds have also been investigated in LbL based OPVs. Up-shifting the LUMO level of the fullerene results in a larger difference between the HOMO level of the donor and the LUMO level of the acceptor, which induces a greater open circuit voltage (*V*<sub>oc</sub>).<sup>15,39</sup> Indene fullerenes such as IC60BA (Fig. 1, a8) and IC70BA (Fig. 1, a9) possess LUMO levels 0.17 eV and 0.19 eV greater than their fullerene counterparts, yielding an increase in *V*<sub>oc</sub> of +0.3 V when incorporated into LbL OPVs.<sup>40</sup> Troshin *et al.* developed

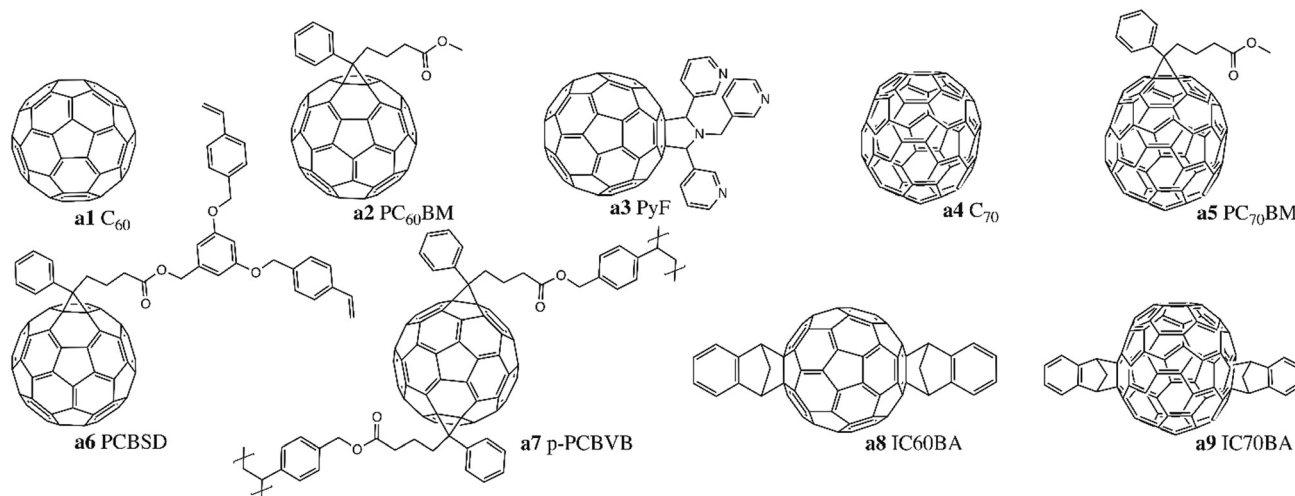


Fig. 1 Chemical structures of select fullerene-based acceptors incorporated into LbL devices.



**Table 1** Energy levels of select fullerene-based acceptors incorporated into LbL devices

| Material                          | HOMO (eV) | LUMO (eV) | Ref. |
|-----------------------------------|-----------|-----------|------|
| C <sub>60</sub> ( <b>a1</b> )     | -6.2      | -4.5      | 63   |
| PC <sub>61</sub> BM ( <b>a2</b> ) | -5.93     | -3.91     | 46   |
| PC <sub>71</sub> BM ( <b>a5</b> ) | -5.87     | -3.91     | 46   |
| IC60BA ( <b>a8</b> )              | —         | -3.74     | 46   |
| IC70BA ( <b>a9</b> )              | -5.61     | -3.72     | 46   |

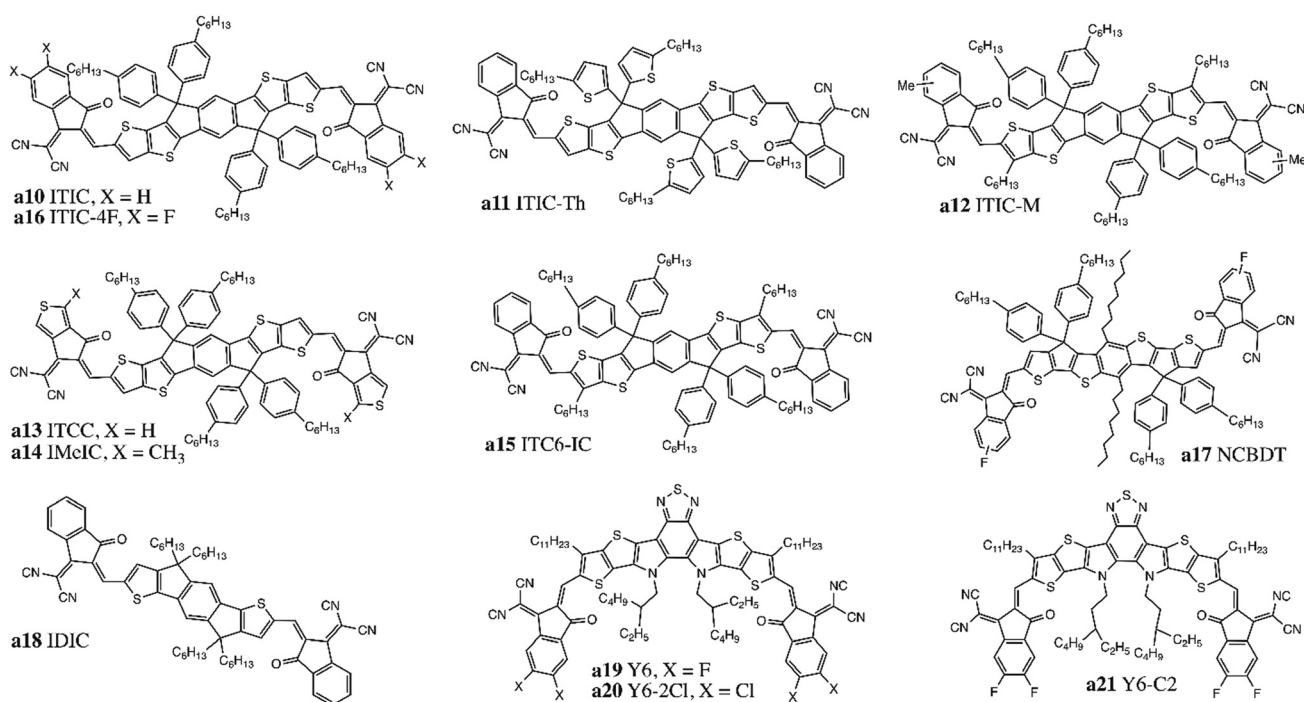
fullerenes bearing chelating pyridyl moieties, such as pyrroli-dinofullerene (PyF) (Fig. 1, **a3**), which can form complexes to increase miscibility with metalloporphyrins and metallophthalocyanines donors, leading to enhanced  $J_{sc}$  compared to PC<sub>61</sub>BM.<sup>41–43</sup> Cross-linked fullerene derivatives bearing two styryl groups for each unit like [6,6]-phenyl-C<sub>61</sub>-butyric acid styryl dendron ester (PCBSD) (Fig. 1, **a6**) and p-PCBVB (Fig. 1, **a7**) have also been studied, and were shown to produce very robust films through LbL (Table 1).<sup>44,45</sup>

## 2.2. Non-fullerene small molecule acceptors

Fullerene derivatives have weak absorption in the visible and near-infrared region of the solar spectrum; the fullerene structure also curtails tuning of the band gap, limiting  $V_{oc}$  values. Additionally, they have a strong tendency to crystallise and form aggregates which reduces device stability.<sup>39,46,47</sup> Non-fullerene acceptors (NFAs) were developed to overcome the impediments of fullerene acceptors. Zhan and coworkers synthesized a novel acceptor, (3,9-bis(2-methylene-(3-(1,1-dicyanomethylene)-indanone))-5,5,11,11-tetrakis(4-hexylphenyl)dithieno[2,3-*d*:2',3'-*d'*]-s-indaceno[1,2-*b*:5,6-*b'*]dithiophene) (ITIC, Fig. 2, **a10**), based on an acceptor-donor-acceptor

(A–D–A) push–pull architecture.<sup>48</sup> The donor core consists of an indacenodithiophene (IDT) unit with four 4-hexylphenyl substituents, while 2-(3-oxo-2,3-dihydroinden-1-ylidene)malononitrile (INCN) was incorporated as the acceptor end groups. Substituents were included to inhibit planarity in the molecule, which would result in excessive  $\pi$ - $\pi$  aggregation and phase separation with donor materials. The A–D–A structure can promote intramolecular charge transfer and strong absorption in the visible spectrum from 500–780 nm. The optical band gap, HOMO and LUMO energy levels were estimated to be 1.59 eV, -5.48 eV and -3.83 eV, respectively. In LbL devices, this novel low band gap NFA achieved a power conversion efficiency (PCE) of 7% when combined with a wide band gap polymer PBDB-T (Fig. 6, **b41**), whose HOMO and LUMO energy levels are -5.33 eV and -3.53 eV, respectively.<sup>49</sup>

In subsequent iterations of the ITIC structure, Zhan and coworkers substituted the phenyl rings of the out-of-plane side-chains on the IDT core with thiophene rings (ITIC-Th, Fig. 2, **a11**) to lower the HOMO level to -5.66 eV to improve compatibility with wider band gap high-performing donor polymers.<sup>50</sup> Small and weakly electron-donating methyl substituents on the phenyl end groups (ITIC-M, Fig. 2, **a12**) were also investigated and found to increase the LUMO level (+0.04 eV) and improve the  $V_{oc}$ .<sup>51</sup> Other strategies focused on replacing the phenyl ring end groups by more electron-donating thiophene rings (ITCC/MeIC, Fig. 2, **a13–14**) or introducing hexyl alkyl chains onto the central fused ring (ITC6-IC, Fig. 2, **a15**), both of which increased the LUMO by +0.11 eV and +0.09 eV, respectively.<sup>52,53</sup> Incorporation of highly electronegative fluorine atoms on the INCN unit ends (ITIC-4F/NCBDT, Fig. 2, **a16–17**) reduced both the HOMO and LUMO levels and narrowed the band gap, particularly for NCBDT ( $E_g = 1.47$  eV).<sup>54–56</sup> Reducing the number of fused ring in the

**Fig. 2** Chemical structures of select non-fullerene acceptors (NFAs) incorporated into LbL devices.

**Table 2** Energy levels of select non-fullerene acceptors (NFAs) incorporated into LbL devices

| Material               | HOMO (eV) | LUMO (eV) | Ref. |
|------------------------|-----------|-----------|------|
| ITIC ( <b>a10</b> )    | -5.48     | -3.83     | 48   |
| ITIC-Th ( <b>a11</b> ) | -5.66     | -3.93     | 50   |
| ITIC-M ( <b>a12</b> )  | -5.58     | -3.98     | 51   |
| ITCC ( <b>a13</b> )    | -5.47     | -3.76     | 52   |
| ITC6-IC ( <b>a15</b> ) | -5.73     | -3.92     | 53   |
| ITIC-4F ( <b>a16</b> ) | -5.73     | -4.02     | 54   |
| NCBDT ( <b>a17</b> )   | -5.36     | -3.89     | 56   |
| Y6 ( <b>a19</b> )      | -5.65     | -4.02     | 60   |
| Y6-2Cl ( <b>a20</b> )  | -5.68     | -4.12     | 60   |

core from seven to five (IDIC, Fig. 2, **a18**) decreased crystallinity and improved phase separation.<sup>57,58</sup> Incorporation of these ITIC based NFAs enabled PCEs greater than 10% when fabricated into LbL OPV devices, with a maximum PCE of 13% obtained for PBDB-TFS1/ITIC-4F devices.<sup>28,59</sup>

Recently, Yuan *et al.* adapted the A-D-A system by replacing the donor core with a new dithienothiophen[3.2-*b*]-pyrrolobenzothiadiazole (TPBT) fused-unit and substituting the INCN acceptor units with fluorine atoms to synthesize (2,2'-(2*Z*,2'*Z*)-((12,13-bis(2-ethylhexyl)-3,9-diundecyl-12,13-dihydro-[1,2,5]thiadiazolo[3,4-*e*]thieno[2'',3'':4',5']thieno[2',3':4,5]pyrrolo[3,2-*g*]thieno[2',3':4,5]-thieno[3,2-*b*]indole-2,10-diyl)bis(methanylylidene))bis(5,6-difluoro-3-oxo-2,3-dihydro-1*H*-indene-2,1-diylidene))dimalononitrile) (Y6, Fig. 2, **a19**).<sup>17</sup> The TPBT core is conjugated, with solubility preserved by incorporation of alkyl chains that can also facilitate tuning of the electron affinity, while end groups promote both photon absorption and intermolecular interactions *via* non-covalent

F-S and F-H bond formation. HOMO and LUMO levels were estimated to be -5.65 eV and -4.02 eV, respectively, and replacement of fluorine atoms with chlorine atoms (Y6-2Cl, Fig. 2, **a20**) further reduced both energy levels and the band gap (-70 meV).<sup>60</sup> Increasing the alkyl chain length on the donor unit (Y6-C2, Fig. 2, **a21**) did not alter optical properties but did improve the molecular packing and enhance crystallinity.<sup>61</sup> LbL processed devices based on these small molecules achieved record efficiencies greater than 16% (Table 2).<sup>31</sup>

### 2.3. Small molecules donors

One of the earliest classes of donor molecules to be utilized in LbL fabrication of OPVs was pentacene, due to the ease with which it can be functionalized to modify hole mobility, solubility, and optical properties.<sup>62,63</sup> Pentacene molecules were first integrated into LbL devices through sublimation, with subsequent reports investigating the use of soluble derivatives such as 6,13-di(2-thienyl)pentacene (BTP, Fig. 3, **b1**), containing two thiophene rings pendent to the central phenyl unit, and bis(triisopropylsilyl)ethynyl)pentacene (TIPS-pentacene, Fig. 3, **b2**) which possesses two alkyl substituted silyl groups. For BTP, a HOMO level of -5.1 eV and a LUMO level of -3.0 eV were reported, with a PCE of 1.4% when paired with C<sub>60</sub>.

Squaraine dyes have attracted significant attention as donor molecules due to their high absorption coefficient (10<sup>5</sup> cm<sup>-1</sup>) in the visible region and tunable band gaps.<sup>64,65</sup> Contrary to NFAs described above, squaraine dyes are based on a donor-acceptor-donor (D-A-D) push-pull structure, with a central four-membered acceptor ring linked to electron-rich moieties such as phenols,

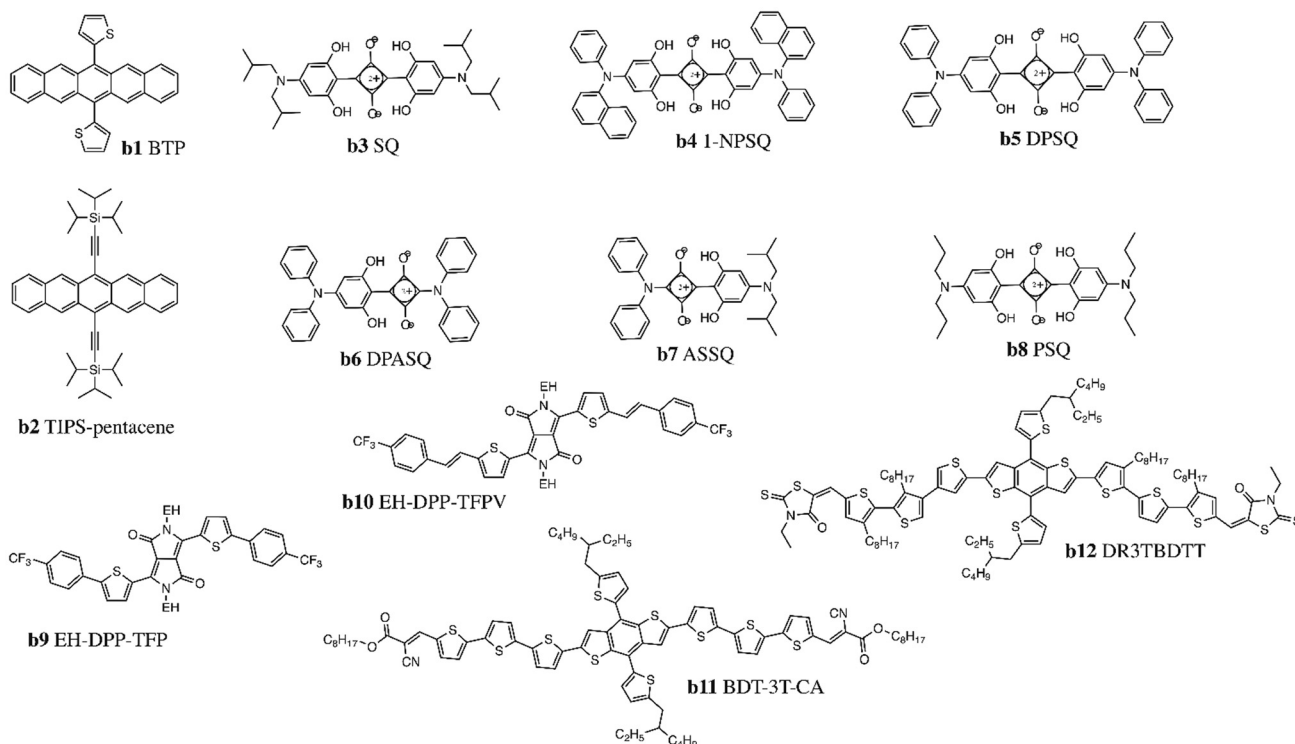


**Fig. 3** Chemical structures of select donor small molecules incorporated into LbL devices.



**Table 3** Energy levels of select donor small molecules incorporated into LbL devices

| Material                 | HOMO (eV) | LUMO (eV) | Ref. |
|--------------------------|-----------|-----------|------|
| BTP ( <b>b1</b> )        | -5.1      | -3.0      | 63   |
| SQ ( <b>b3</b> )         | -5.1      | -3.5      | 66   |
| 1-NPSQ ( <b>b4</b> )     | -5.3      | -3.7      | 66   |
| ASSQ ( <b>b7</b> )       | -5.3      | 3.2       | 66   |
| EH-DPP-TFP ( <b>b9</b> ) | 5.24      | -3.50     | 68   |
| BDT-3T-CA ( <b>b11</b> ) | -5.20     | -2.90     | 71   |

*N,N*-dialkylanilines, or arylamines. The isobutylamine end groups of the initial squaraine derivative 2,4-bis[4-(*N,N*-diisobutylamino)-2,6-dihydroxy-phenyl]squaraine (SQ, Fig. 3, **b3**) were substituted with arylamines (1-NPSQ, DPSQ, DPASQ, ASSQ, Fig. 3, **b4–7**) or *N*-propyl groups (PSQ, Fig. 3, **b8**) to suppress steric hindrance and increase  $\pi$ -stacking between donor molecules; this allows for better hole collection efficiency and stronger electron-withdrawing behavior to improve  $V_{oc}$ .<sup>66</sup> Champion LbL OPV PCE of 5.7% was obtained for the 1-NPSQ paired with a  $C_{60}$  acceptor (Table 3).

Diketopyrrolopyrrole (DPP) dyes are another common class of small molecule donors which possess strong intermolecular interactions and high charge carrier mobilities; their electron-deficient nature also affords them outstanding light harvesting properties.<sup>67</sup> However, the poor solubility of DPP necessitates the incorporation of branched ethyl hexyl alkyl substituents on the nitrogen atoms (EH-DPP-TFP, EH-DPP-TFPV, Fig. 3, **b9–10**) before utilization as donors in LbL devices with PCEs of up to 3.3%.<sup>68</sup>

Chen and coworkers investigated a donor small molecule with an A–D–A structure comprised of an electron-rich benzo-dithiophene (BDT) core linked to alkyl cyanoacetate (BDT-3T-CA, Fig. 3, **b11**) or to ethylrhodanine (DR3TBDTT, Fig. 3, **b12**) through terthiophene spacers.<sup>69,70</sup> When paired with  $PC_{61}BM$ , BDT-3T-CA achieved a PCE of 4.16% with a fill factor (FF) as high as 0.75.<sup>71</sup>

#### 2.4. Ambipolar small molecules

There are several classes of molecules that can be integrated into LbL OPVs as either acceptors or donors, depending on how the molecules are functionalized and the resultant HOMO and LUMO energy levels. Cyanine (Cy) dyes were among the first small molecules investigated as donors with fullerenes in LbL OPV devices, particularly with  $C_{60}$ . These dyes possess high extinction coefficients, tunable absorption spectra, excellent solubility, and suitable HOMO and LUMO energy levels, which motivated their incorporation into OPV cells. Cy dyes also form H and J aggregates with highly delocalized excitons that account both for broaden spectral absorption and larger  $V_{oc}$ . In 2003, Nüesch and coworkers fabricated devices through spin casting a perchlorate counterion, 1,1-diethyl-3,3,3',3'-tetramethyl-carbocyanine perchlorate (Cy3-ClO<sub>4</sub><sup>-</sup>, Fig. 4, **c1**).<sup>72</sup> Subsequent investigations compared this compound to a cyanine derivative with a linked counterion (Cy10, Fig. 4, **c2**), and determined that mobile ions were responsible for an important  $C_{60}$  contribution at the donor/acceptor heterojunction.<sup>73</sup> They also demonstrated that both doping of Cy3-ClO<sub>4</sub><sup>-</sup> in the presence of ambient air increased hole mobility and switching to a hexafluorophosphate counterion (Cy3-PF<sub>6</sub><sup>-</sup>, Fig. 4, **c3**) yielded devices with PCE greater

than 3%.<sup>74,75</sup> Application of Cy as both a donor and an acceptor was achieved through substitution of the phenyl groups for naphthalene rings (CyA, CyBs, CyBl, Fig. 4, **c4–6**), resulting in modified redox levels, with superior performance achieved when used as donors with an hexafluorophosphate counterion (Cy7-P, Fig. 4, **c7**).<sup>76,77</sup> Bolink and coworkers further investigated Cys as donors with different alkyl chains (CyA, Cy0363, Cy2046, Cy0619, Fig. 4, **c4, c8–c10**) and attained PCEs of 3%.<sup>78</sup> A Cy derivative (Cy5-Cl, Fig. 4, **c11**) was also incorporated as a counterion in a polyelectrolyte polymer in an attempt to fabricate an all-solution processed bilayer device with  $PC_{61}BM$  (Table 4).<sup>79</sup>

Porphyrins (Por) are conjugated macrocyclic dyes that have high molar absorptivity (in both the blue and red regions of the visible solar spectrum), excellent air and thermal stability, and efficient photon absorption and electron transfer.<sup>80,81</sup> Por are often integrated as complexes with  $C_{60}$ , but have also been investigated as donors or acceptors in BHJ cells with soluble fullerene derivatives or low band gap polymers. In LbL devices both benzene-functionalized Por and more complex liquid crystalline Por molecules were introduced as donors (BP, PtTPBP, C12/C14Por, Fig. 4, **c12–15**),<sup>82–84</sup> while a Por with quaternized pyridyl side groups (Fig. 4, **c16**) was studied as an acceptor.<sup>85</sup>

Metal phthalocyanines (MPcs), a type of Por, are conjugated macrocycles comprised of four isoindoline groups which chelate a central metal atom. MPcs encompass a wide family of molecules, with a variety of core metals reported; they can also be functionalized both in peripheral and axial positions to tune both electronics and solubility. The most common divalent MPcs, zinc phthalocyanines (ZnPc) and copper phthalocyanines (CuPc) (Fig. 4, **c17–18**), were introduced into LbL devices as donors but efficiencies were low.<sup>43,86</sup> Jones and coworkers synthesized a water-soluble CuPc derivative through the addition of a tetra-sulfonic acid tetrasodium salt substituent on the periphery (TsCuPc, Fig. 4, **c19**), which resulted in a  $V_{oc}$  of 0.6 V.<sup>87</sup> A tetravalent silicon phthalocyanine (SiPc) functionalized in the axial position with fluorophenoxy groups ((246F)<sub>2</sub>/(345F)<sub>2</sub>-SiPc, Fig. 4, **c20–21**) was reported in bilayer cells as an acceptor by Faure *et al.*<sup>88</sup> Bender and coworkers investigated boron subphthalocyanine (SubPc),<sup>89</sup> which consist of a bowl shaped macrocycle chelating a central boron atom, resulting in increased solubility and reduced propensity to aggregate.<sup>90</sup> Josey *et al.* investigated axially-substituted chloro SubPc without and with peripheral chlorination (Cl-BSubPc, Cl-Cl<sub>6</sub>BSubPc, Fig. 4, **c22–c23**) as evaporated acceptors with a standard donor polymer.<sup>89</sup> Soluble SubPc donor derivatives have been synthesized by Fréchet and coworkers, incorporating phenoxy or alkynyl bonded thiophene axial substituents (SubPc-A, 2/4Ta/Tp-SubPc, Fig. 4, **c24–28**) to tune flexibility and molecular packing in the solid state.<sup>91,92</sup> This group also reported a SubPc analogue with similar properties, subnaphthalocyanine (SubNc), obtained by replacing isoindoline by benzoisoindole units (Fig. 4, **c29**).<sup>93</sup> Overall the use of SubPcs and MPcs led to modest PCEs between 1–2% through LbL. Similar boron-based dyes like azadipyrromethene (BO-ADPM, Fig. 4, **c30**) with downshifted HOMO and LUMO levels were reported to give slightly improved PCEs through LbL processing.<sup>94</sup>



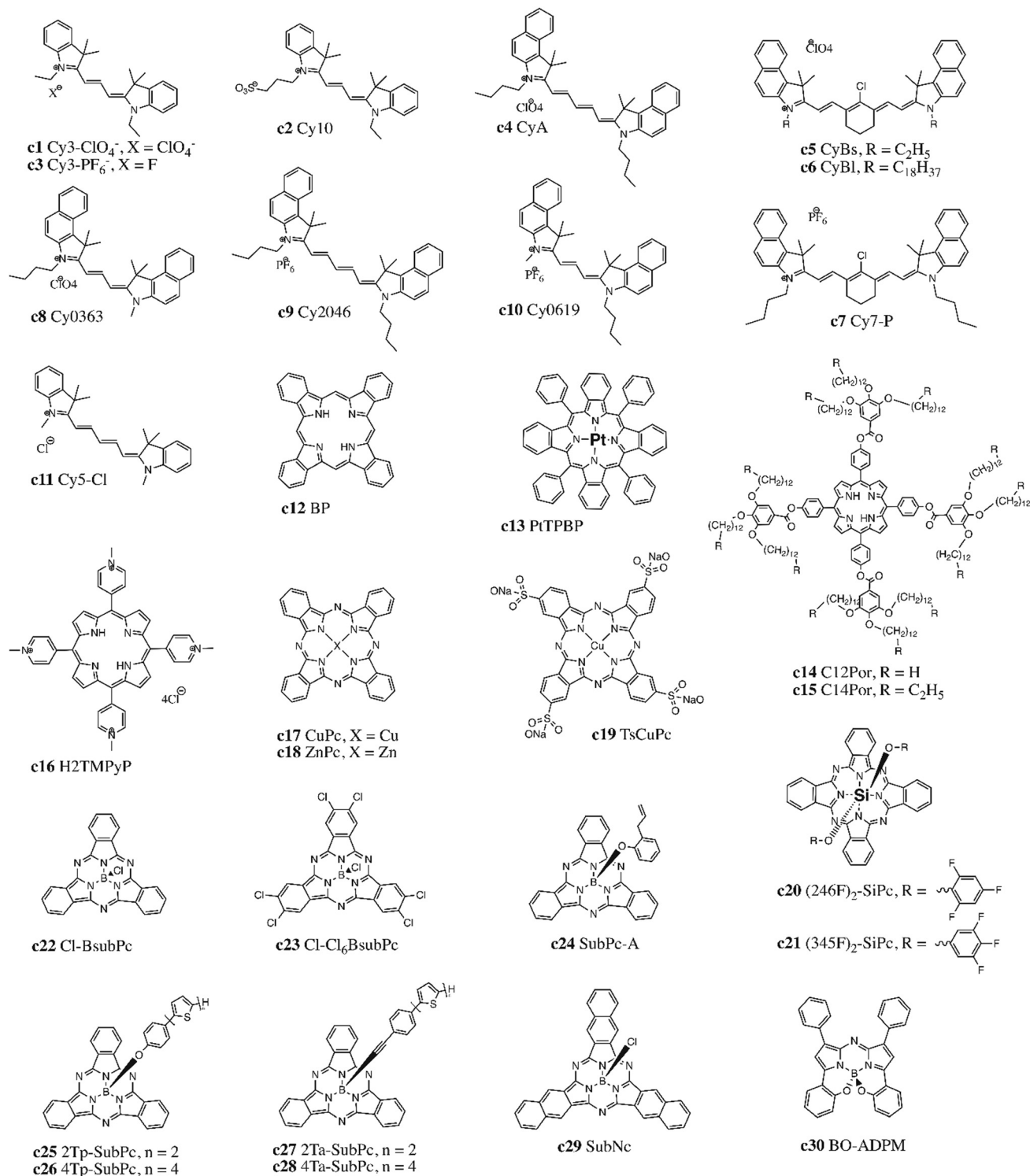


Fig. 4 Chemical structures of select ambipolar small molecules incorporated into LbL devices.

## 2.5. Donor conjugated polymers

In the first iterations of LbL OPV devices, donor polymers were selected to compliment C<sub>60</sub> acceptors. In 1993, Heeger and coworkers prepared LbL devices by spin coating the conjugated polymer poly(2-methoxy,5-(2'-ethyl-hexyloxy)-*p*-phenylenevinylene) (MEH-PPV, Fig. 5, **b13**)<sup>95-97</sup> followed by evaporation of the C<sub>60</sub>

acceptor layer. MEH-PPV is a soluble derivative of poly(*p*-phenylenevinylene) (PPV),<sup>98,99</sup> with a much lower glass transition temperature than PPV; however, it proved to be a weak donor with a relatively wide band gap of 2.2 eV. Drees *et al.* explored the film properties of MEH-PPV films and reported using LbL as a first approach towards fabricating BHJ devices, using a





**Table 4** Energy levels of select ambipolar small molecules incorporated into LbL devices

| Material  | HOMO (eV) | LUMO (eV) | Ref. |
|---|-----------|-----------|------|
| Cy3-ClO <sub>4</sub> <sup>-</sup> ( <b>c1</b> ) | -5.8      | -3.7      | 72   |
| Cy3-PF <sub>6</sub> <sup>-</sup> ( <b>c3</b> )  | -5.7      | -3.9      | 204  |
| CyA ( <b>c4</b> )                               | -5.4      | -3.9      | 76   |
| CyBl/CyBs ( <b>c5/c6</b> )                      | -5.2      | -4.2      | 76   |
| Cy7-P ( <b>c7</b> )                             | -5.28     | -3.79     | 77   |
| C12-Por/C14-Por ( <b>c14/c15</b> )              | -5.4      | -3.3      | 83   |
| CuPc ( <b>c17</b> )                             | -5.06     | -3.35     | 82   |
| (246F) <sub>2</sub> -SiPc ( <b>c20</b> )        | -5.4      | -3.5      | 88   |
| (345F) <sub>2</sub> -SiPc ( <b>c21</b> )        | -5.9      | -4.0      | 88   |
| Cl-BSubPc ( <b>c22</b> )                        | -5.6      | -3.6      | 89   |
| SubNc ( <b>c29</b> )                            | -5.4      | -3.6      | 93   |
| BO-ADPM ( <b>c30</b> )                          | -5.48     | -4.02     | 94   |

concentration gradient of MEH-PPV and C<sub>60</sub> to increase the donor/acceptor interface *via* thermally controlled interdiffusion.<sup>100,101</sup> Another PPV derivative (MDMO-PPV, Fig. 5, **b14**) was also investigated using the same interdiffusion of layers with PC<sub>61</sub>BM as an acceptor and thermal annealing.<sup>102,103</sup> However, overall performances again remained limited (Table 5).

A first approach to increase performances of donor polymers was to replace the phenyl rings with thiophene rings. Schlebusch *et al.* paired C<sub>60</sub> with poly(3-octylthiophene) (P3OT, Fig. 5, **b15**), a soluble thiophene-based polymer with a long alkyl side chain, and discovered that interdiffusion between P3OT and C<sub>60</sub> was occurring even at room temperature.<sup>104</sup> Heflin and coworkers utilized the improved solubility of C<sub>60</sub> in P3OT to pursue the formation of a thermally-induced concentration gradient, and achieved improved active layer morphology with a monochromatic PCE = 1.5%.<sup>105,106</sup> However, the breakthrough in LbL OPV performance occurred with P3HT (Fig. 5, **b16**), which has since become the most researched donor polymer for fullerene acceptors in LbL OPVs. P3HT has a shorter alkyl chain and a lower band gap of 2 eV (HOMO = -5 eV, LUMO = -3 eV) compared to P3OT.<sup>22,107</sup> P3HT also has strong self-organisation capacity, high hole mobility, and strong absorption in the visible region. Moreover, thermal annealing of P3HT near its melting point improves the crystallization of the active layer, resulting in significantly enhanced PCE of 3.5%. A plethora of P3HT derivatives have since been synthesized and integrated into LbL OPVs, including: P3HT-grafted graphene (G-P3HT),<sup>108</sup> poly(3-butylthiophene-2,5-diyl) (P3BT, Fig. 5, **b17**),<sup>109</sup> poly(3-hexyl-2,5-thienylene vinylene) (P3HTV, Fig. 5, **b18**),<sup>110</sup> poly(3-butylthiophene-co-3-octylthiophene)s (RBOs, Fig. 5, **b19**),<sup>111</sup> poly(3-butylthiophene-co-(3-(2-ferrocen-1-yl-vinyl)thiophene)) (P1, Fig. 5, **b20**) and poly(3-butylthiophene-co-(3-(1-cyano-2-ferrocen-1-yl-vinyl)thiophene)) (P2, Fig. 5, **b21**).<sup>109</sup> These modifications in the P3HT donor polymer structure resulted in OPVs with PCEs < 5%. An alternating fluorene and bithiophene copolymer poly(9,9'-dioctyl-fluorene-co-bithiophene) (F8T2, Fig. 5, **b22**) with a band gap of 2.4 eV was studied as well due to its excellent hole transport properties and inherent molecular stacking, resulting in a PCE of 3.4% with C<sub>70</sub>.<sup>112</sup>

Analogous to the BHJ OPV field, significant PCE improvements were achieved in LbL OPVs with the incorporation of low band gap donor polymers, resulting in increased coverage of the solar spectrum compared to P3HT. The so-called

“push-pull” polymers consist of an electron rich unit and an electron deficient unit within the polymer backbone.<sup>5</sup> Monomers are typically fused heterocycles with extended  $\pi$ -conjugation and good planarity to enable tuning of both the band gap and charge carrier mobilities. Some of the most thoroughly investigated electron-rich units include BDT, carbazole (CZ) and cyclopentadithiophene (CPDT), are usually coupled with electron-poor units: DPP, thienothiophene (TT), benzothiadiazole (BTH) or thiazolo(5,4-*d*)thiazole (TzTz). Representative copolymers based on these structures and employed in LbL OPV devices are depicted in Fig. 5, **b23–39**.

Efficiencies of fullerene-based diffused bilayers increased significantly with these push-pull polymers. For example, copolymers based on BDT and TT units (Fig. 5, **b32–36**) including poly[4,8-bis(5-(2-ethylhexyl)thiophen-2-yl)benzo[1,2-*b*;4,5-*b'*]dithiophene-2,6-diyl-*alt*-(4-(2-ethylhexyl)-3-fluorothieno[3,4-*b*]thiophene)-2-carboxylate-2,6-diyl)] (PTB7-Th, Fig. 5, **b33**) have reported PCEs of up to 9% in LbL OPVs.<sup>25</sup> The HOMO and LUMO levels of PTB7-Th are -5.20 eV and -3.59 eV, respectively, with a band gap of 1.61 eV. Another common polymer incorporating CZ and BTH, poly[*N*-9'-heptadecanyl-2,7-carbazole-*alt*-5,5-(4',7'-di-2-thienyl-2',1',3'-benzothiadiazole)] (PCDTBT, Fig. 5, **b26**), as well as copolymers of CPDT with BTH (Fig. 5, **b23–25**), have resulted in PCEs > 7%.<sup>113</sup>

Moving away from fullerene acceptors, these push-pull polymers do not perform well when paired with NFAs due to energy level mismatch. Therefore, to increase the  $J_{sc}$  and  $V_{oc}$  of LbL OPV devices wider band gap (WBG) polymers (> 2 eV) with deeper HOMO levels were designed to be paired with higher-performing emerging NFAs.<sup>114</sup> Representative WBG copolymers employed in LbL OPVs are illustrated in Fig. 6, **b40–51**, and can be divided into two families of copolymers. The first type are donor-donor WBG copolymers, comprised only of alternating electron-rich units in the backbone, such as poly[5,5'-bis(2-butylthiophenyl)-(2,2'-bithiophene)-4,4'-dicarboxylate-*alt*-5,5'-2,2'-bithiophene] (PDCBT, Fig. 6, **b40**).<sup>115</sup> The second class are donor-acceptor copolymers synthesized with alternating electron-rich and electron-poor units in their backbones, including polymers based on a bithienyl-BDT (BBDT) electron-rich unit coupled with a benzodithiophene-4,8-dione (BDD) electron-poor unit (Fig. 6, **b41–43**).<sup>116</sup> Sun *et al.* reported poly[(2,6-(4,8-bis(5-(2-ethylhexyl-3-fluoro)thiophen-2-yl)-benzo[1,2-*b*;4,5-*b'*]dithiophene)-*alt*-(5,5-(1',3'-di-2-thienyl-5',7'-bis(2-ethylhexyl)benzo[1',2'-*c*:4',5'-*c'*]dithiophene-4,8-dione))] (PM6, Fig. 6, **b42**) which achieved a PCE above 16% when paired with Y6 in a LbL OPV device.<sup>31</sup> Other high performing D-A copolymers include poly[(thiophene)-*alt*-(6,7-difluoro-2-(2-hexyldecyloxy)quinoxaline)] (PTQ10, Fig. 6, **b44**), comprised of a simple thiophene ring donor unit and a difluorine-substituted quinoxaline acceptor unit; fluoro and alkoxy substituents are incorporated to lower the HOMO level and ensure sufficient solubility, respectively.<sup>117</sup> J61/J71 (Fig. 6, **b45–46**) are both based on a BBDT electron-rich unit paired with fluorobenzo-triazole (FTAZ) as the electron-deficient unit, with alkylthio or Si-C side chains that further downshift the HOMO level.<sup>118,119</sup> The FTAZ units promote co-planarity in the backbone, resulting in improved  $\pi$ - $\pi$  stacking and overall charge transport properties



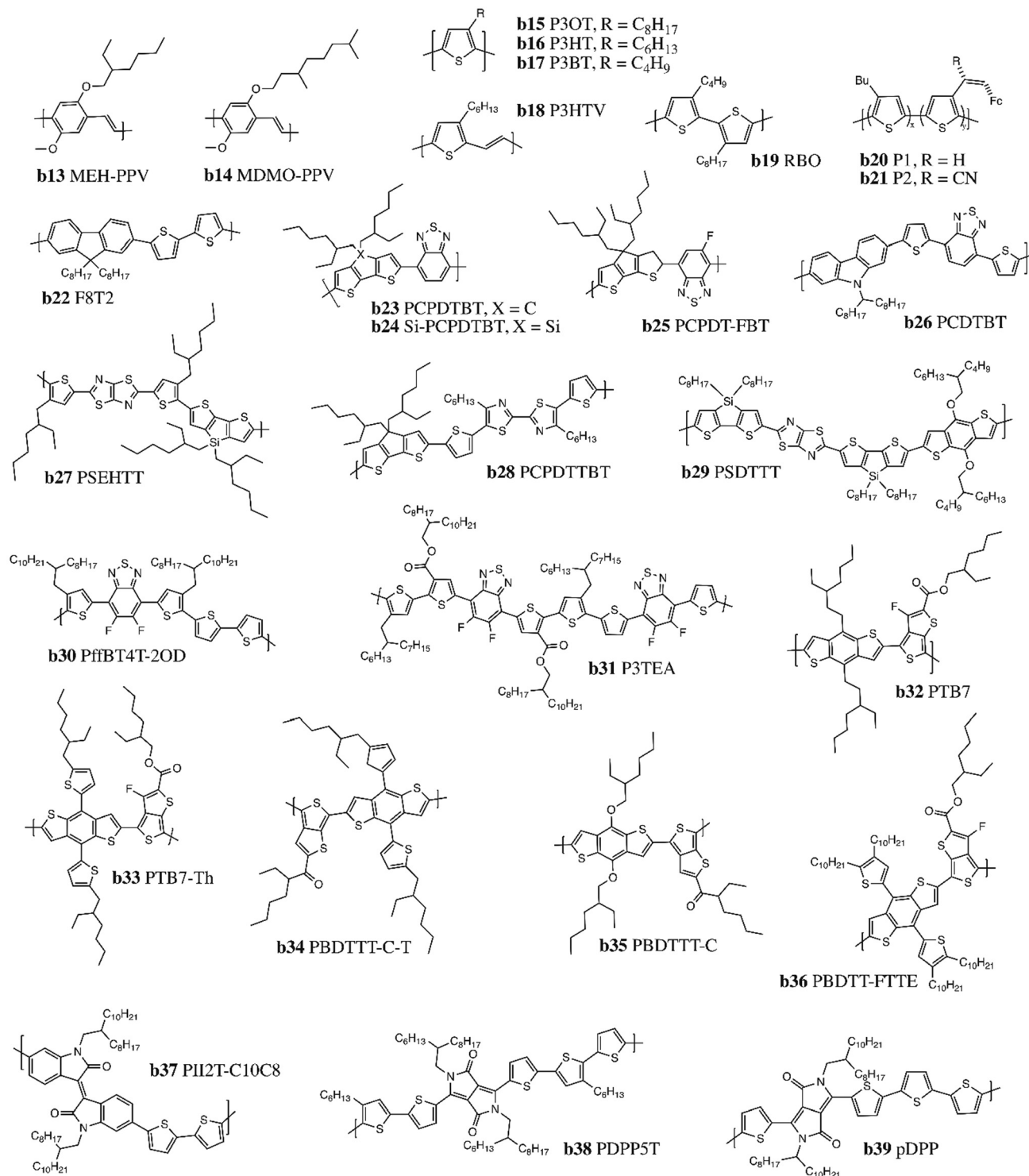


Fig. 5 Chemical structures of common polymer donors (**b13**–**b22**) and low band gap polymer donors (**b23**–**b39**) incorporated into LbL devices.

compared to previously synthesized copolymers (Fig. 6, **b47**/**b49**/**b51**).<sup>120,121</sup> LbL OPV devices based on these copolymers reached PCEs > 12% (Table 6).<sup>28</sup>

## 2.6. Acceptor conjugated polymers

Naphthalenediimide (NDI) based conjugated polymers were among the first acceptor conjugated polymers to be investigated,

due to a low lying LUMO analogous to fullerenes.<sup>122</sup> They have high thermal and oxidative stability, good solubility, favourable electron mobility, and a morphology that can be easily manipulated through side chain engineering with substituents on the bay region or on the nitrogen atom. Jenekhe *et al.* reported the use of poly(benzimidazobenzophenanthroline ladder) (BBL, Fig. 7, **a22**) paired with PPV as the first LbL dual polymer system.<sup>123</sup>



**Table 5** Energy levels of select common polymer donors and low band gap polymer incorporated into LbL devices

| Material                  | HOMO (eV) | LUMO (eV) | Ref. |
|---------------------------|-----------|-----------|------|
| MEH-PPV ( <b>b13</b> )    | -5.1      | -2.9      | 76   |
| P3HT ( <b>b16</b> )       | -5.0      | -3.0      | 88   |
| Si-PCPDTBT ( <b>b24</b> ) | -4.8      | -3.31     | 177  |
| PCDTBT ( <b>b26</b> )     | -5.5      | -3.6      | 88   |
| PTB7-Th ( <b>b33</b> )    | -5.20     | -3.59     | 114  |

**Table 6** Energy levels of representative wider band gap (WBG) polymer donors incorporated into LbL devices

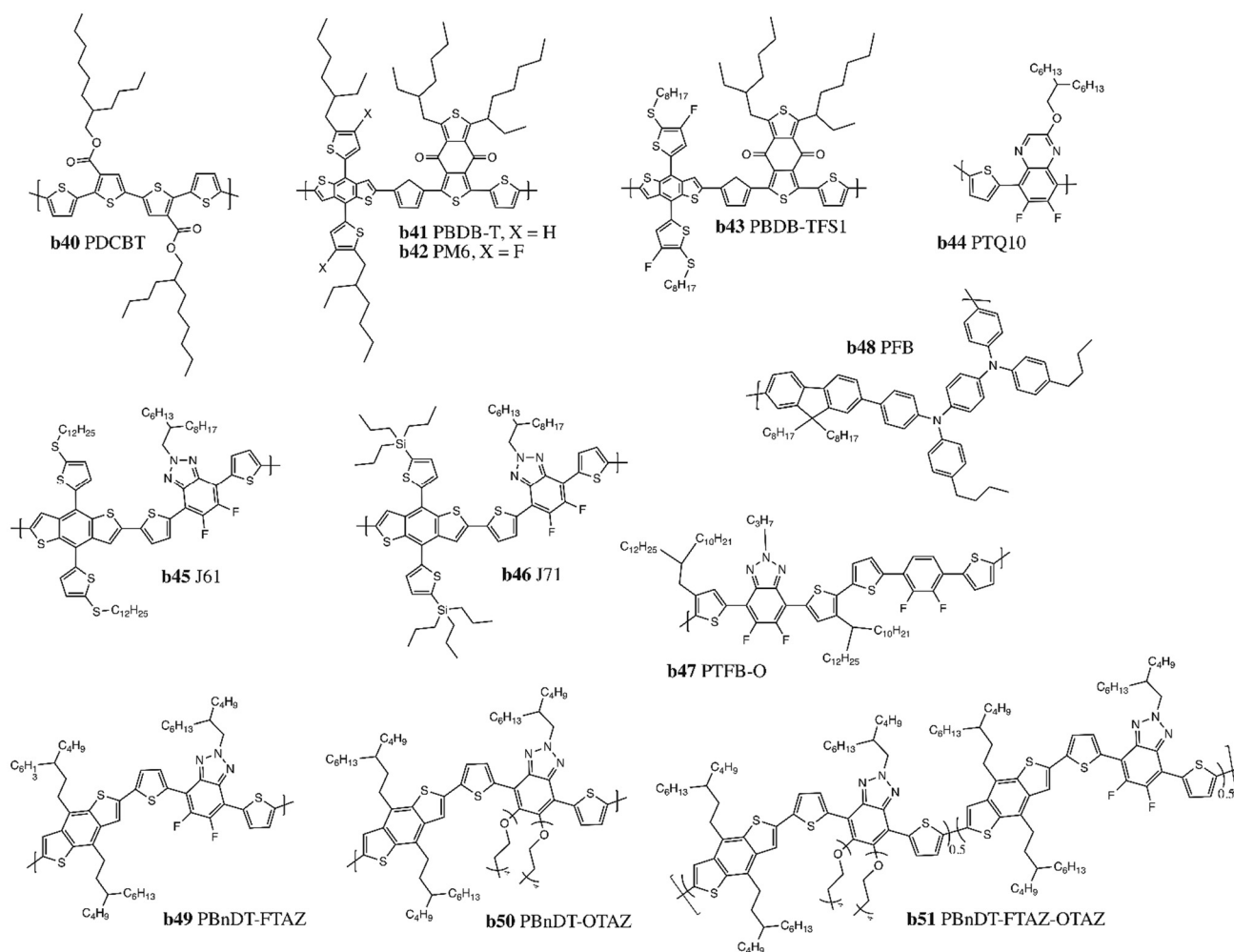
| Material              | HOMO (eV) | LUMO (eV) | Ref. |
|-----------------------|-----------|-----------|------|
| PDCBT ( <b>b40</b> )  | -5.26     | -3.36     | 115  |
| PBDB-T ( <b>b41</b> ) | -5.33     | -3.53     | 51   |
| PM6 ( <b>b42</b> )    | -5.56     | -3.50     | 17   |
| PTQ10 ( <b>b44</b> )  | -5.54     | -2.98     | 117  |
| J61 ( <b>b45</b> )    | -5.32     | -3.08     | 118  |

Poly[*N,N*9-bis(2-octyldodecyl)-naphthalene-1,4,5,8-bis(dicarboximide)-2,6-diyl]-*alt*-5,59-(2,29-bithiophene) (P(NDI2OD-T2) or N2200, Fig. 7, **a23**), is a well established planar push-pull copolymer acceptor containing NDI acceptor and thiophene donor units that is an air-stable n-type semiconductor utilized in organic field-effect transistors (OTFTs), with electron mobility of 0.45–0.85 cm<sup>2</sup> V<sup>-1</sup> s<sup>-1</sup>.<sup>124</sup> Strong interactions between polymer chain backbones, combined with relatively high molecular weights, drastically reduced the solubility of N2200, which facilitated integration into all-polymer LbL OPVs to yield PCE of almost 10% with PBDB-T (Fig. 6, **b41**).<sup>125</sup>

Burn and coworkers recently developed a polymeric acceptor with an acceptor-acceptor'-acceptor (A-A'-A) structure (PNNT,

Fig. 7, **a24**), where NDI was used as the A' unit and thiazole groups as the A units, linked together in an alternating polymer with thiophene units, resulting in decreased LUMO level to -4.3 eV (Table 7).<sup>126</sup>

Another monomeric building block that has been explored for use in polymeric acceptors is perylene diimide (PDI). While PDI is structurally similar to NDI, it has a tendency to form large aggregate domains, promoting separation with the polymer donor and reduced exciton dissociation.<sup>127</sup> PDIs have been evaporated as small molecules, as well as integrated into soluble copolymers for solution processing.<sup>109</sup> Marder and coworkers synthesized a polymer with electron-rich dithienothiophene (DTT) and electron-poor PDI (PPDIDTT, Fig. 7, **a25**) that exhibited

**Fig. 6** Chemical structures of representative wider band gap (WBG) polymer donors incorporated into LbL devices.

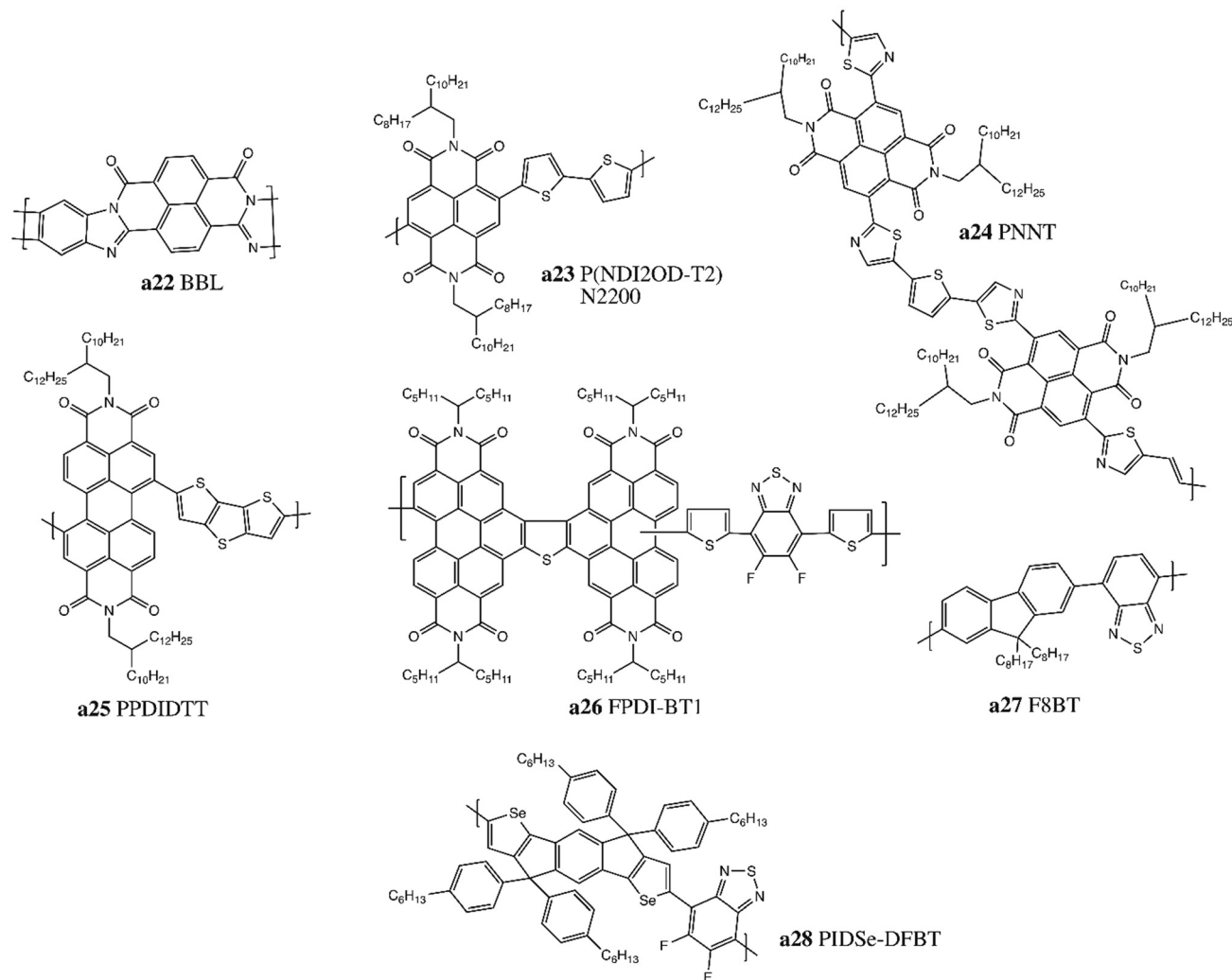


Fig. 7 Chemical structures of representative polymer acceptors incorporated into LbL devices.

Table 7 Energy levels of representative polymer acceptors incorporated into LbL devices

| Material                  | HOMO (eV) | LUMO (eV) | Ref. |
|---------------------------|-----------|-----------|------|
| BBL ( <b>a22</b> )        | -5.9      | -4.0      | 123  |
| N2200 ( <b>a23</b> )      | -5.4      | -3.9      | 124  |
| PNNT ( <b>a24</b> )       | —         | -4.3      | 126  |
| PPDIDTT ( <b>a25</b> )    | -5.9      | -3.9      | 128  |
| PIDSe-DFBT ( <b>a28</b> ) | -5.3      | -3.5      | 133  |

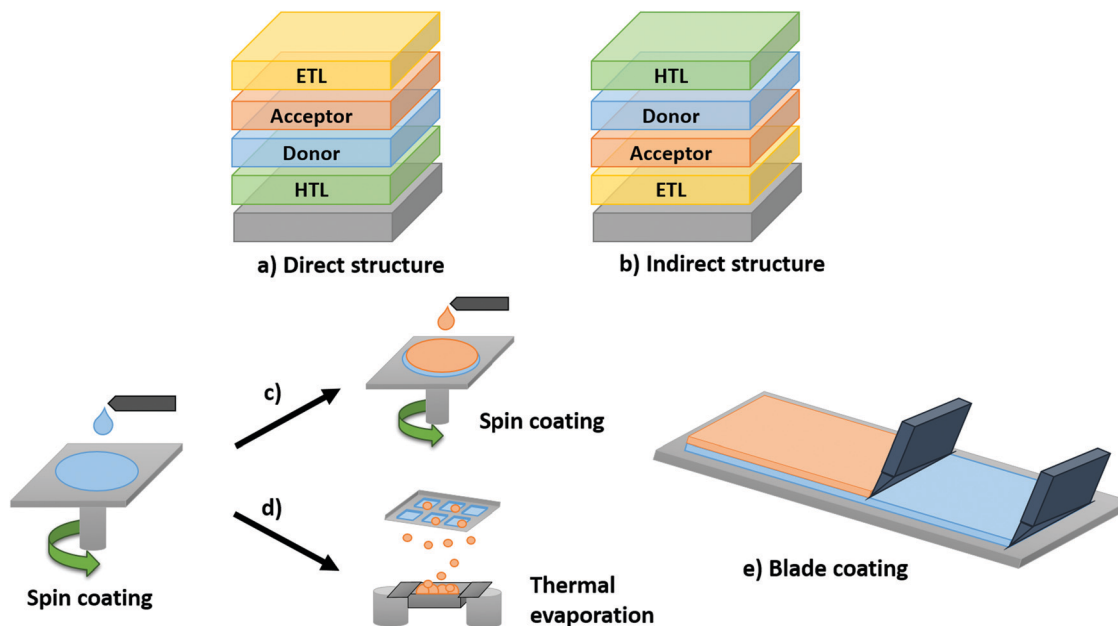
good thermal stability, a LUMO level of  $-3.9$  eV, and a high electron mobility of  $1.3 \times 10^{-2} \text{ cm}^2 \text{ V}^{-1} \text{ s}^{-1}$ .<sup>128</sup> However, when introduced into LbL OPV devices it only resulted in a PCE of 1%.<sup>129</sup> Ade and coworkers developed a rigid, planar copolymer containing two PDI units fused with thiophene moieties to a fluorinated BTH unit (FPDI-BT1, Fig. 7, **a26**).<sup>130</sup> The rigid nature of the backbone, combined with the specific twist angle of the fused PDI dimer, reduced both the formation of large aggregates and the reorganization energy during film formation, producing devices with PCE of  $> 7\%$ .<sup>131</sup> Fluorene and IDT building blocks have also been coupled with BTH units (F8BT, PIDSe-DFBT, Fig. 7, **a27–28**)

leading to favourable electron affinity and good electron mobility but poor performance when integrated into LbL OPV devices.<sup>132,133</sup>

### 3. LbL OPV device fabrication by sequential spin coating processes

The properties of the LbL active layer can be decoupled through separate optimization of the first and the second layers. The first layer is solution processed, and can be annealed prior to deposition of the second layer to yield the desired morphology, crystallinity, and roughness. Deposition of the second layer can be achieved by one of three routes: use of an orthogonal solvent to the first layer (resulting in a bilayer interface), utilizing a compatible solvent (to create a pseudo-bilayer, Scheme 1), or evaporation (Scheme 2c and d). Additional processing and annealing steps can be exploited to enhance interdiffusion of the bilayer or expansion of the pseudo-bilayer.<sup>82,134</sup> Table 8 is a summary of the performance (PCE) and processing conditions for solution-processed LbL OPV devices prepared *via* spin coating,





Scheme 2 Diagram of (a) a direct structure configuration and (b) an indirect structure configuration of OPV devices, and fabrication process via (c) sequential spin coating, (d) hybrid spin coating/thermal evaporation route, (e) blade coating.

with emphasis on material composition, solution concentration, spin rate, and annealing conditions. High-performing devices can only be achieved with optimal intermixing to yield favorable vertical phase separation. Compared to BHJ devices, which produce a random blend of the acceptor and donor materials, the LbL method facilitates superior separation over the entire length of the active layer, promoting improved charge transportation and collection.<sup>23–25,30,71,125,155,178</sup> This vertical active layer separation is often described as a three phase morphology, where a substantial concentration of the donor can be found at the anode, acceptor at the cathode and a blend in the center, enabling LbL solution-processed devices to outperform BHJ devices.

Ayzner *et al.* initially reported the spin casting of P3HT (Fig. 5, **b16**)/PC<sub>61</sub>BM (Fig. 1, **a2**) LbL OPV devices by depositing the donor (P3HT) from *o*-dichlorobenzene (DCB), followed by the acceptor (PC<sub>61</sub>BM) in dichloromethane (DCM), a solvent which does not dissolve the P3HT layer. The authors reported a well-defined planar interface resulting in a PCE of 3.5%, which is comparable to performances obtained with BHJ devices.<sup>22</sup> The P3HT/PC<sub>61</sub>BM system has since been investigated by numerous groups, using a similar methodology to achieve efficiencies comparable or greater than their BHJ counterparts.<sup>24,40,135–154,156–172</sup> The best reported efficiency of this donor/acceptor system in LbL devices is 5.1%, realized by formation of a bicontinuous donor/acceptor network which resulted in significantly reduced bimolecular recombination.<sup>24</sup> However, these literature reports consistently determined that even without optimization of these processing conditions, interdiffusion between P3HT and PC<sub>61</sub>BM was occurring. Despite the use of orthogonal solvents, intermixing between the two materials is transpiring due to swelling of the P3HT layer from the solvent used for the fullerene deposition.<sup>135,139,140,145,191</sup>

Thermal annealing of the bilayer increases the degree of intermixing by inducing miscibility and penetration of PC<sub>61</sub>BM

molecules into the amorphous region of P3HT, without disruption of the ordered polymeric domains.<sup>192</sup> By annealing devices at 150 °C for 20 min, Lee *et al.* increased the PCE from 1.31 to 3.8%.<sup>139</sup>

Cheng *et al.* demonstrated efficient vertical phase separation of PBDTTT-C-T (Fig. 5, **b34**)/PC<sub>61</sub>BM (Fig. 1, **a2**) devices that exhibited an average PCE of 6.86%, exceeding performances measured from analogous BHJ blends (4.31%).<sup>155</sup> Further iterations consisted of substituting PC<sub>61</sub>BM with PC<sub>71</sub>BM (Fig. 1, **a5**) or ICBA (Fig. 1, **a8–9**) fullerene small molecules, paired with lower band gap conjugated polymers, permitting increased efficiencies up to almost 9%.<sup>23,25,26,30,155,173–186</sup>

Recently, NFAs have been integrated into spin casted bilayer devices, enabling PCEs in excess of 10%.<sup>28,29,44,49,59,123,125,126,129,130,133,187–190</sup> One example of a NFA system is PBTB-TFS1 (Fig. 6, **b43**)/ITIC-4F (Fig. 2, **a16**), which was reported to produce a PCE of 13%, surpassing blend-based devices (11.8%).<sup>59</sup> Cui *et al.* demonstrated that solubility and solvent choice are key for high performing LbL OPV devices.<sup>59</sup> Numerous studies have since shown the pseudo-bilayer morphology is susceptible to variations in the solvent or cosolvent,<sup>130,144–146,157,167,168,170,173,175,177,187,189</sup> but is also influenced by other parameters such as thermal annealing,<sup>24,132,134,137,152,153,155,156,160,161,181,184,191,193,194</sup> use of additives,<sup>26,166,168,171,176,180,182</sup> or addition of binary components to the donor polymer.<sup>141,143,148,158,161</sup>

Cho *et al.* explored how solvent choice influenced morphology and phase separation in P3HT layers. Chlorobenzene (CB), DCB, chloroform (CF) and *p*-xylene (*p*-XY) were all investigated for processing the P3HT layer, with *p*-XY also utilized for the PC<sub>61</sub>BM acceptor layer.<sup>146</sup> A PCE around 3% was obtained for *p*-XY, while devices prepared from CB had a PCE of only 0.5%, indicating that the formation and extent of the phase separation is highly influenced by solvents. Similarly, Yi *et al.* investigated CF, toluene (Tol), CB, DCB and 1,2,4-trichlorobenzene (TCB) as solvents for



Table 8 Photovoltaic device properties and processing conditions of LbL OPV devices prepared via spin-coated processes

| Donor/<br>concentration<br>(mg ml <sup>-1</sup> ) | Acceptor/<br>concentration<br>(mg ml <sup>-1</sup> ) | Structure<br>direct (Di) or<br>indirect (In) | Solvent (D) <sup>a</sup> /<br>spin rate (rpm) | Solvent (A)/<br>spin rate (rpm) | Thermal<br>treatment <sup>b</sup><br>(°C min <sup>-1</sup> ) | PCE<br>(%) | Ref. |
|---|--|--|---|---------------------------------|--|------------|------|
| BP (c12)/10                                       | PC <sub>61</sub> BM (a2)/6                           | Di   | CF:CB/—                                       | Tol/3000                        | D: 160/20<br>A: 65/10  | 2.25       | 82   |
| P3OT (b15)/8                                      | PC <sub>61</sub> BM (a2)/20                          | Di   | CF/2750                                       | Pyridine/2450                   | D: 120/10<br>A: 150/20                                       | 1          | 134  |
| P3HT (b16)/20                                     | PC <sub>61</sub> BM (a2)/10                          | Di   | DCB/1000                                      | DCM/4000                        | 150/20   | 3.5        | 22   |
| P3HT (b16)/40 (4 wt%)                             | PC <sub>61</sub> BM (a2)/50 (5 wt%)                  | Di   | CB/—  | DCM/—                           | 150/30   | 2.6        | 135  |
| P3HT (b16)/15                                     | PC <sub>61</sub> BM (a2)/5                           | Di   | DCB/1000                                      | DCM/2000                        | 100/10   | 3.6        | 136  |
| P3HT (b16)/40 (4 wt%)                             | PC <sub>61</sub> BM (a2)/50 (5 wt%)                  | Di   | CB/—  | DCM/—                           | 150/30   | 2.18       | 137  |
| P3HT (b16)/20                                     | PC <sub>61</sub> BM (a2)/5                           | In   | CB/2500                                       | DCM/4500                        | D: 150/10<br>A: 150/5  | 2.6        | 138  |
| P3HT (b16)/15                                     | PC <sub>61</sub> BM (a2)/5                           | Di   | DCB/1000                                      | DCM/4000                        | D: 60/20<br>A: 150/20  | 3.8        | 139  |
| P3HT (b16)/15                                     | PC <sub>61</sub> BM (a2)/5                           | Di   | DCB/1000                                      | DCM/4000                        | 150/5  | 4          | 140  |
| P3HT (b16)/20                                     | PC <sub>61</sub> BM (a2)/5                           | Di   | CB/1500                                       | DCM/4000                        | 150/10   | 3.45       | 141  |
| P3HT:F <sub>4</sub> -TCNQ/20 (0.5 wt%)            | PC <sub>61</sub> BM (a2)/5                           | Di   | CB/1500                                       | DCM/4000                        | 150/10   | 4.02       | 141  |
| P3HT (b16)/30                                     | PC <sub>61</sub> BM (a2)/10                          | Di   | CB/2000                                       | DCM/2000                        | 140/10   | 3.25       | 142  |
| P3HT (b16)/30                                     | PC <sub>61</sub> BM (a2)/10                          | Di   | CB/2500                                       | DCM/4000                        | —  | 3.09       | 143  |
| P3HT:RRa-P3HT/30 (15 wt%)                         | PC <sub>61</sub> BM (a2)/10                          | Di   | CB/2500                                       | DCM/4000                        | —  | 3.83       | 143  |
| P3HT (b16)/—                                      | PC <sub>61</sub> BM (a2)/—                           | Di   | DCB/—   | DCM/—                           | 140–180/30   | 3.93       | 144  |
| P3HT (b16)/—                                      | PC <sub>61</sub> BM (a2)/—                           | Di   | CB/—  | DCM/—                           | 150/10   | 3.45       | 145  |
| P3HT (b16)/15 (1.5 wt%)                           | PC <sub>61</sub> BM (a2)/15 (1.5 wt%)                | Di   | <i>p</i> -XY/1000                             | <i>p</i> -XY/1000               | 150/3  | 2.70       | 146  |
| P3HT (b16)/22                                     | PC <sub>61</sub> BM (a2)/—                           | Di   | DCB/900                                       | DCM/3000                        | 150/20   | 4.12       | 40   |
| P3HT (b16)/30                                     | PC <sub>61</sub> BM (a2)/10                          | Di   | CB/2500                                       | DCM/4000                        | 140/10   | 3.81       | 147  |
| P3HT (b16)/—                                      | PC <sub>61</sub> BM (a2)/5 (0.5 wt%)                 | Di   | CB/2000                                       | DCM/—                           | 180/20   | 2.8        | 148  |
| P3HT:PEG/— (6 wt%)                                | PC <sub>61</sub> BM (a2)/5 (0.5 wt%)                 | Di   | CB/2000                                       | DCM/—                           | 180/20   | 3.71       | 148  |
| P3HT (b16)/—                                      | PC <sub>61</sub> BM (a2)/—                           | Di   | CB/—  | DCM/—                           | —  | 1.80       | 149  |
| P3HT (b16)/20                                     | PC <sub>61</sub> BM (a2)/5                           | Di   | DCB/700                                       | DCM/3000                        | D: 140/—<br>A: 120/10  | 3.39       | 150  |
| P3HT (b16)/10                                     | PC <sub>61</sub> BM (a2)/5                           | Di   | DCB/1000                                      | DCM/4000                        | 140/30   | 1.8        | 151  |
| P3HT (b16)/—                                      | PC <sub>61</sub> BM:PEG/— (5 wt%)                    | Di   | DCB/—   | DCM/3000                        | 150/20   | 4.40       | 152  |
| P3HT (b16)/15                                     | PC <sub>61</sub> BM (a2)/5                           | Di   | DCB/1000                                      | DCM/4000                        | D: 90/5<br>A: 150/20   | 3.25       | 153  |
| P3HT (b16)/15                                     | PC <sub>61</sub> BM (a2)/5                           | Di   | DCB/1000                                      | DCM/4000                        | D: 60/20<br>A: 150/20  | 3.24       | 154  |
| PCDTBT (b26)/7                                    | PC <sub>61</sub> BM (a2)/10                          | Di   | DCB/700                                       | DCM/4000                        | —  | 4.27       | 23   |
| PBDTTT-C-T (b34)/15                               | PC <sub>61</sub> BM (a2)/8                           | Di   | DCB/—   | DCM/—                           | 110/30   | 6.86       | 155  |
| P3HT (b16)/20                                     | PC <sub>61</sub> BM (a2)/—                           | Di   | DCB/1000                                      | DCM/4000                        | 150/20   | 3.4        | 156  |
| P3HT (b16)/5                                      | PC <sub>61</sub> BM (a2)/10                          | Di   | CF/—  | DCM/—                           | —  | 2.16       | 157  |
| P3HT (b16)/30                                     | PC <sub>61</sub> BM (a2)/10                          | Di   | CB/2500                                       | —/4000                          | 140/10   | 3.09       | 158  |
| P3HT:PS/30  | PC <sub>61</sub> BM (a2)/10                          | Di   | CB/2500                                       | —/2000                          | 140/10   | 3.25       | 158  |
| P3HT:RRa-P3HT/30 (15 wt%)                         | PC <sub>61</sub> BM (a2)/10                          | Di   | CB/2500                                       | —/4000                          | 140/10   | 3.83       | 158  |
| BDT-3T-CA (b11)/7.5                               | PC <sub>61</sub> BM (a2)/—                           | Di   | CF/—  | DCM/3500                        | —  | 4.16       | 71   |
| P3HT (b16)/20                                     | PC <sub>61</sub> BM (a2)/10                          | Di   | DCB/1000                                      | DCM/4000                        | 150/20   | 2.97       | 159  |
| P3HT (b16)/15                                     | PC <sub>61</sub> BM (a2)/4                           | Di   | CB/1000                                       | DCM/4000                        | 150/20   | 3.54       | 160  |
| Cy5-Cl (c11)/2                                    | PC <sub>61</sub> BM (a2)/—                           | Di   | TFP/—   | CB/—                            | —  | 0.93       | 79   |
| P3HT:TES-ADT/20 (5 wt%)                           | PC <sub>61</sub> BM (a2)/10                          | Di   | CB/—  | DCM/4000                        | 150/1  | 2.70       | 161  |
| P3HT (b16)/—                                      | PC <sub>61</sub> BM (a2)/5                           | Di   | DCB/1000                                      | DCM/350 + 4000                  | D: 50/5<br>A: 150/20   | 5.1        | 24   |
| P3HT (b16)/15                                     | PC <sub>61</sub> BM (a2)/4                           | Di   | CB/1000                                       | DCM/4000                        | 150/20   | 3.71       | 162  |
| P3HT (b16)/20                                     | PC <sub>61</sub> BM (a2)/10                          | Di   | DCB/—   | DCM/—                           | 150/30   | 2.79       | 163  |
| P3HT (b16)/—                                      | PC <sub>61</sub> BM (a2)/—                           | Di   | DCB/—   | DCM/4000                        | —  | 3.11       | 164  |
| P3HT (b16)/12                                     | PC <sub>61</sub> BM (a2)/8                           | Di   | DCB/1000                                      | DCM/800                         | D: 70/10   | 1.96       | 165  |
| P3HT (b16)/14                                     | PC <sub>61</sub> BM (a2)/3.5                         | Di   | CB:1-CN/1000                                  | DCM/2000                        | D: 110/60  | 3.25       | 166  |
| P3HT (b16)/10                                     | PC <sub>61</sub> BM (a2)/10                          | Di   | CB/1000                                       | Tol:2-CP/—                      | 150/10   | 3.1        | 167  |
| PTB7 (b32)/10                                     | PC <sub>61</sub> BM (a2)/10                          | Di   | CB/1000                                       | 1-Butanol:2-CP/—                | —  | 6.0        | 167  |
| PSDTT (b29)/10                                    | PC <sub>61</sub> BM (a2)/10                          | Di   | CB/1000                                       | Tol:2-CP/—                      | —  | 3.8        | 167  |
| P3HT (b16)/30                                     | PC <sub>61</sub> BM (a2)/—                           | Di   | CB:s-TCB/2500                                 | DCM/4000                        | 140/10   | 3.30       | 168  |
| P3HT (b16)/10                                     | PC <sub>61</sub> BM (a2)/6.4                         | Di   | DCB/—   | DCM/—                           | 150/10   | 2.0        | 169  |
| P3HT (b16)/—                                      | PC <sub>61</sub> BM (a2)/5                           | Di   | Tol/—   | DCM/4000                        | 150/1  | 3.25       | 170  |
| P3HT (b16)/20                                     | PC <sub>61</sub> BM (a2)/10                          | Di   | DCB:DIO/1000                                  | DCM/4000                        | 150/15   | 1.84       | 171  |
| PSEHTT (27b)/10                                   | PC <sub>61</sub> BM (a2)/10                          | Di   | DCB:DIO/2200                                  | DCM/4000                        | 150/15   | 4.13       | 171  |
| PBDTTT-C (b16)/10                                 | PC <sub>61</sub> BM (a2)/10                          | Di   | DCB:DIO/2000                                  | DCM/4000                        | 150/15   | 5.33       | 171  |
| P3HT (b16)/5                                      | PC <sub>61</sub> BM (a2)/5                           | Di   | CF/5000                                       | DCM/2500                        | —  | 0.3        | 172  |
| PCDTBT (b26)/7                                    | PC <sub>71</sub> BM (a5)/28                          | Di   | DCB:CB/5000                                   | DCM:DCB:CB/2000                 | 80/10  | 6.34       | 173  |
| PCDTBT (b26)/7                                    | PC <sub>71</sub> BM (a5)/28                          | Di   | DCB/700                                       | DCM:DCB:CB/4000                 | —  | 5.29       | 23   |
| P3HT (b16)/22                                     | PC <sub>71</sub> BM (a5)/—                           | Di   | DCB/900                                       | DCM/3000                        | 150/20   | 4.38       | 40   |
| PCDTBT (b26)/4                                    | PC <sub>71</sub> BM (a5)/16                          | Di   | CB/—  | DCM/5000                        | —  | 2.11       | 174  |
| PII2T-C10C8 (b37)/7                               | PC <sub>71</sub> BM (a5)/—                           | Di   | CF/—  | DCB/—                           | D: 150/30<br>A: 110/10                                       | 5.02       | 175  |



Table 8 (continued)

| Donor/<br>concentration<br>(mg ml <sup>-1</sup> ) | Acceptor/<br>concentration<br>(mg ml <sup>-1</sup> ) | Structure<br>direct (Di) or<br>indirect (In) | Solvent (D) <sup>a</sup> /<br>spin rate (rpm) | Solvent (A)/<br>spin rate (rpm)   | Thermal<br>treatment <sup>b</sup><br>(°C min <sup>-1</sup> ) | PCE<br>(%) | Ref. |
|---|--|--|---|-----------------------------------|--|------------|------|
| PCDTBT ( <b>b26</b> )/8                           | PC <sub>71</sub> BM ( <b>a5</b> )/6                  | Di   | CB:DIO/2500                                   | DCM:DIM/4000                      | 100/15   | 7.12       | 176  |
| Si-PCPDTBT ( <b>b24</b> )/10                      | PC <sub>71</sub> BM ( <b>a5</b> )/20                 | Di   | DCB/2000                                      | DCM:DCB/2000                      | 120/10   | 4.6        | 177  |
| pDPP ( <b>b39</b> )/5                             | PC <sub>71</sub> BM ( <b>a5</b> )/30                 | Di   | CF:DCB/1000                                   | DCB/—                             | —  | 7.59       | 178  |
| PDPP5T ( <b>b38</b> )/6                           | PC <sub>71</sub> BM ( <b>a5</b> )/24                 | Di   | CF/—  | DCB/—                             | —  | 5.0        | 179  |
| PTB7-Th ( <b>b33</b> )/10                         | PC <sub>71</sub> BM ( <b>a5</b> )/—                  | Di   | DCB/—   | DCM/—                             | —  | 8.5        | 25   |
| PCDTBT ( <b>b26</b> )/10                          | PC <sub>71</sub> BM ( <b>a5</b> )/6                  | Di   | CB:DIO/2500                                   | DCM:DIO/4000                      | D: 110/15, 150<br>A: 110/15                                  | 5.03       | 180  |
| PCPDT-FBT ( <b>b25</b> )/6                        | PC <sub>71</sub> BM ( <b>a5</b> )/16                 | In   | <i>o</i> -XY/—                                | <i>o</i> -XY:DCB/—                | 110/30   | 5.84       | 181  |
| PCPDTBT ( <b>b23</b> )/8                          | PC <sub>71</sub> BM ( <b>a5</b> )/5                  | Di   | CB:DIO/2200                                   | DCM:DPE/1500                      | D: 110/15<br>A: 110/15                                       | 3.36       | 182  |
| PTB7 ( <b>b32</b> )/14                            | PC <sub>71</sub> BM ( <b>a5</b> )/3.25               | Di   | CB:DIO:1-CN/1000                              | DCM/4000                          | —  | 7.43       | 26   |
| PfFBT4T-2OD ( <b>b30</b> )/—                      | PC <sub>71</sub> BM ( <b>a5</b> )/—                  | Di   | XY/—  | XY/—                              | 100/—  | 8.9        | 30   |
| PfFBT4T-2OD ( <b>b30</b> )/10                     | PC <sub>71</sub> BM ( <b>a5</b> )/10                 | Di   | CB/—  | CB/—                              | D: 80/10<br>A: 150/1.5                                       | 7.64       | 183  |
| P3HT ( <b>b16</b> )/22                            | IC60BA ( <b>a8</b> )/7.5                             | Di   | DCB/900                                       | DCM/3000                          | 150/20   | 6.22       | 40   |
| P3HT ( <b>b16</b> )/22                            | IC70BA ( <b>a9</b> )/7.5                             | Di   | DCB/900                                       | DCM/3000                          | 150/20   | 6.48       | 40   |
| P3HT ( <b>b16</b> )/15                            | IC60BA ( <b>a8</b> )/5                               | Di   | DCB/1000                                      | DCM/3000                          | 150/20   | 5.12       | 184  |
| P3HT ( <b>b16</b> )/22.5                          | IC60BA ( <b>a8</b> )/7.4                             | Di   | DCB/2200                                      | DCM/3000                          | 140/50   | 5.6        | 185  |
| P3HT-NW/24  | IC60BA ( <b>a8</b> )/10                              | Di   | DCB/800                                       | DCM/3000                          | D: 140/10<br>A: 150/30                                       | 3.64       | 186  |
| DR3TBDTT ( <b>b12</b> )/—                         | PCBSD ( <b>a6</b> )/—                                | In   | CF/—  | DCB/—                             | A: 170/40  | 1.1        | 44   |
| PPV/—   | BBL ( <b>a22</b> )/—                                 | Di   | MeOH/—  | GaCl <sub>3</sub> :nitromethane/— | D: 250/60<br>A: 40/600                                       | 0.7        | 123  |
| P3HT ( <b>b16</b> )/4                             | PIDSe-DFBT ( <b>a28</b> )/7.5                        | In   | DCM:CB/1500                                   | DCB/1000                          | 140/10   | 2.34       | 133  |
| SQ ( <b>b3</b> )/7                                | PPDIDTT ( <b>a25</b> )/8                             | In   | DCM/—   | DCB/800                           | 100/1  | 1.08       | 129  |
| PBDB-TFS1 ( <b>b43</b> )/10                       | ITIC-4F ( <b>a16</b> )/—                             | Di   | CB/—  | DCB:THF/—                         | 100/10   | 13         | 59   |
| PTB7 ( <b>b32</b> )/10.5                          | N2200 ( <b>a23</b> )/12                              | In   | DCM:CB/2600                                   | DCB:CB/1200                       | —  | 2.94       | 187  |
| PBDIT-FTTE ( <b>b36</b> )/6                       | PNNT ( <b>a24</b> )/6                                | In   | DCB/1000                                      | DCB/1000                          | —  | 4.1        | 126  |
| PBDB-T ( <b>b41</b> )/6                           | NCBDT ( <b>a17</b> )/6                               | Di   | CF/1900                                       | DCM/2500                          | —  | 10.04      | 188  |
| PBDB-T ( <b>b41</b> )/6                           | ITIC ( <b>a10</b> )/6                                | Di   | CF/1900                                       | DCM/2500                          | —  | 5.86       | 188  |
| PTB7-Th ( <b>b33</b> )/6                          | NCBDT ( <b>a17</b> )/6                               | Di   | CF/1900                                       | DCM/2500                          | —  | 8.27       | 188  |
| PTB7-Th ( <b>b33</b> )/6                          | ITIC ( <b>a10</b> )/6                                | Di   | CF/1900                                       | DCM/2500                          | —  | 7.13       | 188  |
| PDCBT ( <b>b40</b> )/6                            | NCBDT ( <b>a17</b> )/6                               | Di   | CF/1900                                       | DCM/2500                          | —  | 3.28       | 188  |
| PDCBT ( <b>b40</b> )/6                            | ITIC ( <b>a10</b> )/6                                | Di   | CF/1900                                       | DCM/2500                          | —  | 2.38       | 188  |
| PM6 ( <b>b42</b> )/—                              | ITIC-4F ( <b>a16</b> )/—                             | Di   | XY/—  | XY/—                              | 100/—  | 12.5       | 30   |
| FTAZ ( <b>b49</b> )/5                             | ITIC-M ( <b>a12</b> )/10                             | Di   | LM/1000                                       | 2-MeTHF/2000                      | 150/10   | 12.2       | 189  |
| OTAZ ( <b>b50</b> )/5                             | ITIC-M ( <b>a12</b> )/10                             | Di   | LM/1000                                       | 2-MeTHF/2000                      | 150/10   | 4.7        | 189  |
| FTAZ-OTAZ ( <b>b51</b> )/5                        | ITIC-M ( <b>a12</b> )/10                             | Di   | LM/1000                                       | 2-MeTHF/2000                      | 150/10   | 5.8        | 189  |
| PTFB-O ( <b>b44</b> )/10                          | ITIC-Th ( <b>a11</b> )/—                             | Di   | CB/2000                                       | THF/—                             | 100/10   | 11.8       | 29   |
| P3TEA ( <b>b31</b> )/12                           | ITIC-4F ( <b>a16</b> )/—                             | Di   | 1,2,4-trimethyl-<br>benzene/2000              | THF/—                             | 100/10   | 9.80       | 29   |
| PBDB-T ( <b>b41</b> )/8                           | ITIC ( <b>a10</b> )/10                               | In   | CB/1500                                       | <i>o</i> -XY/2000                 | —  | 6.7        | 49   |
| PBDB-T ( <b>b41</b> )/7                           | FPDI-BT1 ( <b>a26</b> )/—                            | Di   | DCB/1000                                      | CB:DCB/3500                       | —  | 6.93       | 130  |
| J71 ( <b>b46</b> )/12                             | ITC6-IC ( <b>a15</b> )/12                            | Di   | CF/2000                                       | CF/2000                           | 150/5  | 12.08      | 28   |
| PTQ10 ( <b>b44</b> )/12                           | IDIC ( <b>a18</b> )/12                               | Di   | CF/4000                                       | CF/4000                           | 140/5  | 12.32      | 28   |
| J71 ( <b>b46</b> )/12                             | MeIC ( <b>a14</b> )/12                               | Di   | CF/2000                                       | CF/2000                           | 150/2  | 11.43      | 28   |
| J71 ( <b>b46</b> )/12                             | ITCC ( <b>a13</b> )/12                               | Di   | CF/2000                                       | CF/2000                           | 150/2  | 10.44      | 28   |
| J71 ( <b>b46</b> )/12                             | ITIC ( <b>a10</b> )/12                               | Di   | CF/3500                                       | CF/3500                           | 150/10   | 10.94      | 28   |
| PBDB-T ( <b>b41</b> )/6                           | NCBDT ( <b>a17</b> )/6                               | In   | CF/1900                                       | DCM/2500                          | —  | 10.62      | 190  |
| PBDB-T ( <b>b41</b> )/4                           | N2200 ( <b>a23</b> )/4                               | In   | CF/2000                                       | CB/2000                           | —/10   | 9.52       | 125  |

<sup>a</sup> Solvent acronyms: chlorobenzene (CB), 1,2-dichlorobenzene (DCB), chloroform (CF), *p*-xylene (*p*-XY), toluene (Tol), 1,2,4-trichlorobenzene (TCB), (*R*)-(+)-limonene (LM), 2-methyltetrahydrofuran (2-MeTHF), diiodooctane (DIO), 1,8-octanedithiol (ODT). <sup>b</sup> Non-existent step or value not reported designated with “—”.

P3HT, while using DCM to process PC<sub>61</sub>BM.<sup>170</sup> P3HT solutions prepared from low boiling point solvents formed films with reduced crystallinity and numerous amorphous regions, promoting better fullerene diffusion and faster interdiffusion. Kim *et al.* also reported that modification of the processing solvent for PC<sub>61</sub>BM induces a change in the molecular orientation of polymer crystallite from edge-on to more isotropic in PII2T-C10C8 (Fig. 5, **b37**) films, improving vertical charge transportation.<sup>175</sup>

Non-halogenated solvents have also been investigated. Ye *et al.* used (*R*)-(+)-limonene (LM) for FTAZ-based donors (Fig. 6, **b49–51**),

and 2-methyltetrahydrofuran (2-MeTHF) for the ITIC-M (Fig. 2, **a12**) acceptor.<sup>189</sup> LM promoted molecular order in amorphous FTAZ polymer films, facilitating the formation of larger domain spacing and enabling an efficiency of 12.2%, again outperforming BHJ control blends (11.7%). To reach 13% PCE, Cui *et al.* controlled both the bulk interface and nanoscale phase separation by employing specific ratios of cosolvents (DCB:tetrahydrofuran (THF)) for the ITIC-4F film deposition.<sup>59</sup> Comparable improved nanoscale phase separation was also demonstrated by Ahn *et al.*, with controlled penetration of the acceptor through adjustment of



the DCM:DCB cosolvent ratio for PC<sub>61</sub>BM.<sup>177</sup> Cosolvents also facilitate interdiffusion by optimizing the degree of polymer swelling (without dissolving the layer), as reported by Aguirre *et al.* who used a blend of Tol and 2-chlorophenol (2-CP).<sup>167</sup>

Solvent additives can also be exploited to tune the vertical phase separation. Vohra *et al.* used a high-boiling point solvent (*o*-TCB) as an additive for CB solutions of P3HT, which resulted in increased P3HT crystallinity leading to reduced PCBM interdiffusion and thinner intermixed region.<sup>168</sup> On the contrary, low vapor pressure solvents such as diiodooctane (DIO) or 1,8-octanedithiol (ODT) act as polymer swelling agents when incorporated as additives, enabling improved mixing between fullerenes and the polymer, enhancing performances.<sup>171</sup> However, the need for orthogonal solvent, cosolvents or solvent additives in LbL devices is not critical for all combinations of donors and acceptors. For example, Sun *et al.* explored five different donor/acceptor pairs, J71 (Fig. 6, **b46**)/ITC6-IC (Fig. 2, **a15**), PTQ10 (Fig. 6, **b44**)/IDIC (Fig. 2, **a18**), J71/MeIC (Fig. 2, **a14**), J71/ITCC (Fig. 2, **b13**) and J71/ITIC (**a10**), using only CF as a solvent for the sequential spin casting.<sup>28</sup> Fabricated LbL devices systematically exhibited similar or greater efficiencies (10.44–12.32%) than their BHJ blend counterparts (10.46–11.75%), with improved vertical phase separation, stronger absorption spectra, increased charge transport and collection, and reduced energy loss. Dong *et al.* investigated the use of halogen-free xylene (XY) as a solvent for the deposition of PM6 (Fig. 6, **b42**)/ITIC-4F bilayers.<sup>30</sup> The graded separation of layers was preserved, while simultaneously reducing dependence on processing conditions and improving performances compared to BHJ control devices.

Another strategy to tune film morphology is the addition of a binary component to the donor layer. Doping of P3HT with p-type solution-processable small molecules such as tetrafluoro-tetracyanoquinodimethane (F<sub>4</sub>-TCNQ) and 5,11-bis(triethylsilylethynyl)anthradithiophene (TES-ADT) impacts aggregate formation, crystallinity and mobility.<sup>141,161</sup> Film nanostructures can also be controlled through the addition of polyethylene glycol (PEG) or polystyrene (PS) in P3HT solutions.<sup>148,158</sup> After extraction of the PS or PEG, the resulting P3HT films contain porous circular depressions whose diameter and depth can be controlled by modification of the polymer ratios during film deposition. Optimization of the PEG content up to 6 wt% increased the PCE from 2.80 to 3.71% for P3HT/PC<sub>61</sub>BM devices. Regioregular P3HT blended with less crystalline regiorandom P3HT (RRa-P3HT) promotes intermixing and control of the vertical concentration gradient with PC<sub>61</sub>BM.<sup>158</sup> An optimal content of 15 wt% RRa-P3HT improved the PCE from 3.09 to 3.83%.

## 4. Other processing methods

### 4.1. Hybrid spin casting/evaporation process

The use of all-solution processing for LbL devices necessitates that both donor and acceptor materials are sufficiently soluble to be processed. However, many small molecule acceptors, such as C<sub>60</sub> and C<sub>70</sub> (Fig. 1, **a1**, **a4**), are highly insoluble. In such cases a combination of solution processing and thermal

evaporation is employed. The insoluble acceptor is deposited *via* thermal evaporation, with the donor polymer or small molecule layer formed through spin casting to facilitate formation of the bilayer (Scheme 2d). This hybrid route of LbL OPV fabrication enabled the incorporation of C<sub>60</sub> and C<sub>70</sub> acceptors with donor polymers or soluble small molecule such as ADPM, cyanines, squaraines and porphyrins.<sup>62,63,66,68,72,73,75,77,78,83,84,86,87,91–101,104–108,110,112,166,194–207</sup>

Some examples of evaporated phthalocyanine-based NFAs have also been reported.<sup>88,109,208</sup> A summary of device performances and processing conditions from hybrid LbL OPVs prepared from thermally evaporated acceptors can be found in Table 9.

Thermal annealing of hybrid LbL films can induce interpenetration of the donor and the acceptor by promoting diffusion of fullerenes, improving the degree of crystallization and creating a controlled gradient concentration within the active layer.<sup>68,100,101,106,107,110,112,196,206</sup> Early studies involving P3HT (Fig. 5, **b16**)/C<sub>60</sub> (Fig. 1, **a1**) devices demonstrated that annealing the bilayer near the melting point of P3HT (220 °C) produced an intercalated BHJ-like morphology along the interface and enhanced P3HT crystallinity, resulting in PCE values that were an order of magnitude larger compared to the untreated bilayer.<sup>107</sup> However, Stevens *et al.* demonstrated that reducing this annealing temperature results in higher PCE. Heating P3HT/C<sub>60</sub> devices above 190 °C could induce P3HT to migrate to the top surface, while C<sub>60</sub> penetrated into the P3HT amorphous regions, reducing the concentration gradient and negatively impacting PCE values.<sup>110</sup> Annealing at a lower temperature of 170 °C resulted in devices with a PCE of 1.19%.

Huang *et al.* investigated the impact of both pre-annealing and post-annealing on PCPDTTBT (Fig. 5, **b28**)/C<sub>70</sub> (Fig. 1, **a4**) devices.<sup>206</sup> Pre-annealing the bottom PCPDTTBT layer at 200 °C resulted in a fibrillar morphology with increased donor/acceptor interfacial area and an improved PCE of 1.65%. Further post-annealing of the entire bilayer at 200 °C induced nanostructural transformations that reorganized the PCPDTTBT and C<sub>70</sub> interface, expanding the contact area and improving the PCE to 2.85%. Kekuda *et al.* demonstrated that post-annealing of F8T2 (Fig. 5, **b22**)/C<sub>70</sub> hybrid devices at 200 °C increased the PCE from 0.40 to 3.40% due to the creation of an interdigitated structure with well-aligned polymer crystal nanodomain features.<sup>112</sup> The extent of nanocrystalline morphology in 1-NPSQ (Fig. 3, **b4**)/C<sub>60</sub> hybrid devices was also improved through annealing, resulting in an enhanced PCE of 5.7%.<sup>66</sup>

Solvent choice for processing the first layer can also drastically influence interface morphology and significantly improve PCE. Kekuda *et al.* used CF, XY, DCB and 1,2,4-trichlorobenzene (TCB) for P3HT deposition, producing donor films with surface roughness values of 1.14, 4.83, 8.62 and 9.2 nm, respectively.<sup>207</sup> Solvent-induced crystallinity of the polymer, along with increased surface roughness, improved the PCE of P3HT/C<sub>70</sub> hybrid devices from 1.04% (for CB) to 3.56% (for TCB), without a thermal treatment step.

Finally, improved active layer morphology can also be achieved with dopants in the solution-processed layer. The nanostructure of P3HT was modified through blending with graphene (G-P3HT, Table 9) followed by ultrasonic vibration post-treatment of the G-P3HT film, leading to a PCE of 5.17% when paired with





Table 9 Photovoltaic properties and processing conditions of selected hybrid processed LbL OPV devices

| Donor/concentration (mg ml <sup>-1</sup> )                            | Donor solvent/spin rate (rpm) | Acceptor evaporated/thickness (nm)          | Thermal treatment <sup>a</sup> (°C min <sup>-1</sup> ) | PCE (%) | Ref. |
|---|-------------------------------|---|--|---------|------|
| MEH-PPV ( <b>b13</b> )/2  | XY/—                          | C <sub>60</sub> ( <b>a1</b> )/40            | 170/—  | 0.92    | 196  |
| P3HTV ( <b>b18</b> )/15   | DCB/—                         | C <sub>60</sub> ( <b>a1</b> )/40            | 170/20   | 1.19    | 110  |
| P3HT ( <b>b16</b> )/5   | CB/2000                       | C <sub>60</sub> ( <b>a1</b> )/40            | 150/30   | 2.6     | 197  |
| G-P3HT/—  | DMF:CB/—                      | C <sub>60</sub> ( <b>a1</b> )/6             | 140/15   | 5.17    | 205  |
| SubNc ( <b>c29</b> )/—  | CB/2000                       | C <sub>60</sub> ( <b>a1</b> )/35.5          | 120/40   | 1.47    | 93   |
| SubPc-A ( <b>c24</b> )/6  | CB/2000                       | C <sub>60</sub> ( <b>a1</b> )/32            | —  | 1.71    | 91   |
| 2Tp-SubPc ( <b>c25</b> )/3  | CB/2000                       | C <sub>60</sub> ( <b>a1</b> )/32            | —  | 1.39    | 92   |
| Cy3-ClO <sub>4</sub> <sup>-</sup> :NOBF <sub>4</sub> ( <b>c1</b> )/10 | CB/—                          | C <sub>60</sub> ( <b>a1</b> )/40            | —  | 2.0     | 199  |
| Cy0619 ( <b>c10</b> )/7   | CB/1000                       | C <sub>60</sub> ( <b>a1</b> )/30            | —  | 2.5     | 78   |
| Cy3-PF <sub>6</sub> <sup>-b</sup> ( <b>c3</b> )/—                     | TFP/—                         | C <sub>60</sub> ( <b>a1</b> )/—             | —  | 3.7     | 203  |
| BO-ADPM ( <b>c30</b> )/2  | THF/2000                      | C <sub>60</sub> ( <b>a1</b> )/45            | —  | 2.53    | 94   |
| SQ ( <b>b3</b> )/1  | CF/3000                       | C <sub>60</sub> ( <b>a1</b> )/40            | 90/—   | 4.6     | 66   |
| DPSQ ( <b>b5</b> )/1  | CF/3000                       | C <sub>60</sub> ( <b>a1</b> )/40            | 80/—   | 5.2     | 66   |
| 1-NPSQ ( <b>b4</b> )/1  | CF/3000                       | C <sub>60</sub> ( <b>a1</b> )/40            | 70/—   | 5.7     | 66   |
| PCDTBT ( <b>b26</b> )/8   | DCB/2000                      | C <sub>60</sub> ( <b>a1</b> )/              | —  | 1.48    | 88   |
| F8T2 ( <b>b22</b> )/20  | TCB/2000                      | C <sub>70</sub> ( <b>a4</b> )/40            | 200/60   | 3.40    | 112  |
| P3HT ( <b>b16</b> )/—   | TCB/2000                      | C <sub>70</sub> ( <b>a4</b> )/40            | D: 100/60<br>A:150/30                                  | 3.56    | 207  |
| PCPDTTBT ( <b>b28</b> )/10  | TCB/2500                      | C <sub>70</sub> ( <b>a4</b> )/40            | D: 200/60<br>A: 200/60                                 | 2.85    | 206  |
| P3HT ( <b>b16</b> )/15  | DCB/1000                      | Cl-Cl <sub>6</sub> BsubPc ( <b>c23</b> )/20 | —  | 0.52    | 208  |
| P3HT ( <b>b16</b> )/15  | DCB/1000                      | Cl-BsubPc ( <b>c22</b> )/20                 | —  | 0.98    | 208  |
| PCDTBT ( <b>b26</b> )/8   | DCB/2000                      | (345F) <sub>2</sub> -SiPc ( <b>c21</b> )/93 | 150/30   | 1.52    | 88   |

<sup>a</sup> Non-existent step or value not reported designated with “—”. <sup>b</sup> Indirect structure.

C<sub>60</sub>.<sup>205</sup> Doping is also utilized to increase the donor layer conductivity, such as NOBF<sub>4</sub> doped Cy3-ClO<sub>4</sub><sup>-</sup> (Fig. 4, **c1**).<sup>75,199</sup>

## 4.2. Blade coating

One of the core objectives of OPV research is to develop large-scale, roll-to-roll manufacturing of devices. It is therefore essential to transition away from lab-scale spin coating and focus on scalable solution-processing techniques. The majority of high-performing OPV devices have been fabricated from spin coating methods, with the adaptation to industrial printing techniques non-trivial, as minimization of the geometric fill factor (GFF) losses inherent to any type of PV technology is complex.<sup>209</sup> Compared to BHJ OPVs, performances of LbL-processed OPVs have proven to be less dependent on processing conditions, which is often the first barrier encountered.<sup>30</sup>

Some preliminary examples of BHJ OPV devices fabricated using roll-to-roll compatible deposition techniques have been reported, such as slot coating<sup>210–214</sup> or blade coating.<sup>215–220</sup> However, analogous investigations employing LbL processes using similar scalable techniques remain limited. Initial reports focused on hybrid processing, where the first layer was deposited through blade coating.<sup>179,221</sup> Investigations involving deposition of both layers *via* blade coating (Scheme 2e) were only reported in 2019.<sup>28,30,31,222</sup> A summary of device performance and processing conditions for LbL OPVs fabricated from blade coating can be found in Table 10.

Impressive PCEs of >16% have been achieved through blade coating using a combination of NFAs and a single solvent system.<sup>31</sup> Additionally, authors have consistently reported improved performances for LbL-based devices compared to analogous BHJ-based devices. Sun *et al.* attained a PCE of 11.47% for 0.04 cm<sup>2</sup> J71 (Fig. 6, **b46**)/ITC6-IC (Fig. 2, **a15**) LbL OPV blade coated cells using CF as a

solvent for both layers, which was superior to BHJ OPVs prepared from blade coating (10.41%).<sup>222</sup> Detailed characterization of film morphology revealed that LbL blade coating achieved a more thermodynamically favourable nanomorphology, with suitable donor/acceptor interfaces and larger separation between donor/acceptor domains, which was facilitated through independent optimization of each layer. Furthermore, the 3D geometry of the bilayer enabled higher charge generation, increasing the light absorption coefficient. Creation of a well-defined bicontinuous network with a p-i-n like structure also facilitated highways for charge transport and collection at the appropriate electrodes, reducing the rate of charge recombination. Improved photo, thermal, and bending stability compared to the BHJ OPVs was also observed due to the vertical phase separation achieved in LbL devices.

Dong *et al.* fabricated larger area (1 cm<sup>2</sup>) LbL OPVs based on PM6 (Fig. 6, **b42**)/ITIC-4F (Fig. 2, **a16**) using xylene as a non-halogenated processing solvent, and observed similar device performance improvements compared to the BHJ OPV analogues. Advantages with the LbL system included better graded separation of donor and acceptor materials, resulting in an improved PCE of 11% and enhanced photo-stability.<sup>30</sup>

The ubiquity of blade coating processing for LbL OPVs was demonstrated by Sun *et al.*, who performed a comprehensive investigation involving multiple bilayer donor/acceptor systems and compared them to their BHJ OPV equivalents.<sup>28,31</sup> LbL OPVs were prepared from J71 (Fig. 6, **b46**)/ITC6-IC (Fig. 2, **a15**), PTQ10 (Fig. 6, **b44**)/IDIC (Fig. 2, **a18**), PTQ10/Y6 (Fig. 2, **a19**), PM6/Y6, PM6/Y6-2Cl (Fig. 5, **a20**) and PM6/Y6-C2 (Fig. 5, **a21**), with areas ranging from 0.04 to 11.86 cm<sup>2</sup>. For 0.04 cm<sup>2</sup> cells with Y6 derivatives, PCE values above 15% were systematically achieved, with a maximum PCE of 16.4% for PM6/Y6 LbL OPVs,



Table 10 Photovoltaic properties and processing conditions of blade coated LbL OPV devices

| Donor/<br>concentration<br>(mg ml <sup>-1</sup> ) | Solvent (D)/blade<br>spin (mm s <sup>-1</sup> )/<br>blade height (μm) | Acceptor/<br>concentration<br>(mg ml <sup>-1</sup> ) | Solvent (A)/blade<br>spin (mm s <sup>-1</sup> )/<br>blade height (μm) | Thermal<br>annealing <sup>a</sup><br>(°C min <sup>-1</sup> ) | Cell area<br>(cm <sup>2</sup> ) | PCE   | Ref. |
|---|---|--|---|--|---------------------------------|-------|------|
| PBDTTT-C-T <sup>b</sup> (b34)/9                   | Tol:0-XY/200/—  | C <sub>70</sub> (a4)/N/A (Evap)                      | N/A   | —  | 0.05                            | 6.23  | 221  |
| PTB7 <sup>b</sup> (b32)/9                         | Tol:0-XY/—  | C <sub>70</sub> (a4)/N/A (Evap)                      | N/A   | —  | 0.05                            | 7.15  | 221  |
| PDPP5T (b38)/6                                    | CF/N/A (spin coating)   | PC <sub>71</sub> BM (a5)/20                          | TMB/20/254  | —  | 0.09                            | 5.3   | 179  |
| J71 (b46)/12                                      | CF/18/—   | ITC6-IC (a15)/12                                     | CF/18/—   | 150/5  | 0.04                            | 11.47 | 222  |
| PfFBT4T-2OD (b30)/—                               | XY/6/400  | PC <sub>71</sub> BM (a5)/—                           | XY/6/400  | —  | 0.04                            | 8.2   | 30   |
| PfFBT4T-2OD (b30)/—                               | XY/6/400  | PC <sub>71</sub> BM (a5)/—                           | XY/6/400  | —  | 1                               | 7.8   | 30   |
| PM6 (b42)/—                                       | XY/6/400  | ITIC-4F (a16)/—                                      | XY/6/400  | —  | 0.04                            | 11.9  | 30   |
| PM6 (b42)/—                                       | XY/6/400  | ITIC-4F (a16)/—                                      | XY/6/400  | —  | 1                               | 11.0  | 30   |
| J71 (b46)/12                                      | CF/—/400  | ITC6-IC (a15)/12                                     | CF/—/400  | —  | 0.04                            | 11.42 | 28   |
| J71 (b46)/12                                      | CF/—/400  | ITC6-IC (a15)/12                                     | CF/—/400  | —  | 1                               | 10.35 | 28   |
| PTQ10 (b44)/12                                    | CF/—/400  | IDIC (a18)/12  | CF/—/400  | —  | 0.04                            | 11.28 | 28   |
| PTQ10 (b44)/12                                    | CF/—/400  | IDIC (a18)/12  | CF/—/400  | —  | 1                               | 10.42 | 28   |
| PTQ10 (b44)/8                                     | CF/12/—   | Y6 (a19)/8   | CF/12/—   | —  | 0.04                            | 15.10 | 31   |
| PM6 (b42)/8                                       | CF/12/—   | Y6-2Cl (a20)/8                                       | CF/12/—   | —  | 0.04                            | 15.89 | 31   |
| PM6 (b42)/8                                       | CF/12/—   | Y6-C2 (a21)/8  | CF/12/—   | —  | 0.04                            | 15.93 | 31   |
| PM6 (b42)/8                                       | CF/12/—   | Y6 (a19)/8   | CF/12/—   | —  | 0.04                            | 16.35 | 31   |
| PM6 (b42)/8                                       | CF/12/—   | Y6 (a19)/8   | CF/12/—   | —  | 3.3                             | 13.88 | 31   |
| PM6 (b42)/8                                       | CF/12/—   | Y6 (a19)/8   | CF/12/—   | —  | 11.52                           | 11.86 | 31   |

<sup>a</sup> Non-existent step or value not reported designated with “—”. <sup>b</sup> Indirect structure.

which exceeded the BHJ OPV module (15.4%). When the active area was increased to 11.52 cm<sup>2</sup>, the GFF for the same LbL system was over 90% and delivered a PCE of 11.86% compared to 10.15% for BHJ; this represents the superlative reported PCE so far for large-area OPV devices. These promising results demonstrate that LbL blade-coating is an easy and efficient strategy for the up-scaling of OPVs towards future industrial applications.

## 5. Conclusion and perspective

Layer-by-layer (LbL) processing has become increasingly popular as a promising alternative to the widely adopted blended bulk heterojunction (BHJ) process for fabricating the donor/acceptor active layer in high-performing OPVs. In this review, we systematically explored the current literature associated with LbL OPVs, with particular focus on the various donor and acceptor materials utilized and processing conditions. We highlight advances in materials structure and thin film morphology which have resulted in significant improvements in PCE, and how state-of-the-art LbL OPVs consistently outperform their BHJ counterparts.

LbL processing is superior to BHJ blending in numerous ways. Firstly, each layer can be deposited separately and sequentially, enabling independent control and optimization of parameters, such as viscosity, temperature and deposition speed. Each layer can be characterized *in situ* prior to the disposition of the subsequent layer, facilitating optimization and device fabrication troubleshooting, both of which are significant challenges in BHJ blends. Secondly, LbL enables the formation of a graded vertical phase separation between the donor and the acceptor, which is believed to be the preminent morphology for OPV devices. This vertical separation results in improved OPV performance through an interpenetrated bicontinuous network, where accumulation of

each component is greatest at its respective desired electrode, providing sufficient interfacial area for charge separation, optimal percolation pathways for charge transport, and reduced charge recombination. Compared to the BHJ blend process, LbL processing is easier to optimize through modification of processing conditions such as choice of solvents, incorporation of additives and dopants, deposition rate, and annealing steps, resulting in significantly improved fabrication reproducibility. Finally, the LbL approach produces cells with better thermal, mechanical and optical stability over cells fabricated from the BHJ blend technique, which makes LbL more attractive for scaling of modules and eventual industrial fabrication of OPVs. To date, LbL processing has produced the most significant power conversion efficiency retention when transitioning from lab-scale to large-scale devices. Despite these significant advantages, application of LbL remains limited compared to blended BHJ processing. Many researchers gravitate towards the BHJ approach, resulting in the majority of record efficiencies obtained from this technique, perpetuating its dominance in the literature.

As new higher-performing OPV materials and systems are developed, the popularity of the LbL approach is expected to grow. Recent reports of significant improvements in PCE (currently > 16%) and the advancement of LbL OPV fabrication with scalable techniques such as blade coating further underscore the importance of this technology. Larger systematic studies that compare various processing conditions and incorporate different materials using LbL blade coating are still necessary. Furthermore, implementation into roll-to-roll compatible techniques such as gravure and flexography need to be explored to fully assess this technology and facilitate a truly comparison to the standard BHJ blended processing. Overall, LbL is emerging as a promising alternative to BHJ blending for OPV fabrication, but more work is required to establish if it is truly the favoured approach.



## Conflicts of interest

There are no conflicts to declare.

## Acknowledgements

B. H. L. would like to acknowledge financial support from Natural Science and Engineering Research Council of Canada (NSERC) and Canada Research Chair (CRC) programs.

## References

- D. Hengevoss, C. Baumgartner, G. Nisato and C. Hugli, Life Cycle Assessment and Eco-Efficiency of Prospective, Flexible Tandem Organic Photovoltaic Module, *Sol. Energy*, 2016, **137**, 317–327, DOI: 10.1016/j.solener.2016.08.025.
- S. Lizin, S. Van Passel, E. De Schepper, W. Maes, L. Lusten, J. Manca and D. Vanderzande, Life Cycle Analyses of Organic Photovoltaics: A Review, *Energy Environ. Sci.*, 2013, **6**, 3136–3149, DOI: 10.1039/c3ee42653j.
- Q. Liu, Y. Jiang, K. Jin, J. Qin, J. Xu, W. Li, J. Xiong, J. Liu, Z. Xiao, K. Sun, S. Yang, X. Zhang and L. Ding, 18% Efficiency Organic Solar Cells, *Sci. Bull.*, 2020, 1–10, DOI: 10.1016/j.scib.2020.01.001.
- G. A. Chamberlain, Organic Solar Cells: A Review, *Sol. Cells*, 1983, **8**, 47–83, DOI: 10.1016/0379-6787(83)90039-X.
- R. C. Jemison and R. D. McCullough, Techniques for the Molecular Design of Push-Pull Polymers towards Enhanced Organic Photovoltaic Performance, *ACS Symp. Ser.*, 2014, **1161**, 71–109, DOI: 10.1021/bk-2014-1161.ch004.
- C. Yan, S. Barlow, Z. Wang, H. Yan, A. K. Y. Jen, S. R. Marder and X. Zhan, Non-Fullerene Acceptors for Organic Solar Cells, *Nat. Rev. Mater.*, 2018, **3**(18003), 1–19, DOI: 10.1038/natrevmats.2018.3.
- C. W. Tang, Two-Layer Organic Photovoltaic Cell, *Appl. Phys. Lett.*, 1986, **48**(2), 183–185, DOI: 10.1063/1.96937.
- O. V. Mikhnenko, P. W. M. Blom and T. Nguyen, Exciton Diffusion in Organic Semiconductors, *Energy Environ. Sci.*, 2015, **8**, 1867–1888, DOI: 10.1039/c5ee00925a.
- B. C. J. Brabec, N. S. Sariciftci and J. C. Hummelen, Plastic Solar Cells\*\*, *Adv. Funct. Mater.*, 2001, **11**(1), 15–26, DOI: 10.1002/1616-3028(200102)11:1 <15::AID-ADFM15>3.0.CO;2-A.
- M. T. Dang, L. Hirsch and G. Wantz, P3HT:PCBM, Best Seller in Polymer Photovoltaic Research, *Adv. Mater.*, 2011, **23**(31), 3597–3602, DOI: 10.1002/adma.201100792.
- O. Oklobia and T. S. Shafai, A Study of Donor/Acceptor Interfaces in a Blend of P3HT/PCBM Solar Cell: Effects of Annealing and PCBM Loading on Optical and Electrical Properties, *Solid-State Electron.*, 2013, **87**, 64–68, DOI: 10.1016/j.sse.2013.05.005.
- B. Gholamkhash and P. Servati, Solvent-Vapor Induced Morphology Reconstruction for Efficient PCDTBT Based Polymer Solar Cells, *Org. Electron.*, 2013, **14**(9), 2278–2283, DOI: 10.1016/j.orgel.2013.05.014.
- Z. He, B. Xiao, F. Liu, H. Wu, Y. Yang, S. Xiao, C. Wang, T. P. Russell and Y. Cao, Single-Junction Polymer Solar Cells with High Efficiency and Photovoltage, *Nat. Photonics*, 2015, **9**(3), 174–179, DOI: 10.1038/nphoton.2015.6.
- J. Zhao, Y. Li, G. Yang, K. Jiang, H. Lin, H. Ade and H. Yan, Efficient Organic Solar Cells Processed from Hydrocarbon Solvents, *Nat. Energy*, 2016, **1**(15027), 1–7, DOI: 10.1038/NENERGY.2015.27.
- F. B. Kooistra, J. Knol, F. Kastenberg, L. M. Popescu, W. J. H. Verhees, J. M. Kroon and J. C. Hummelen, Increasing the Open Circuit Voltage of Bulk-Heterojunction Solar Cells by Raising the LUMO Level of the Acceptor, *Org. Lett.*, 2007, **9**(4), 551–554, DOI: 10.1021/ol062666p.
- Z. Xu, F. Pan, C. Sun, S. Hong, S. Chen, C. Yang, Z. Zhang, Y. Liu, T. P. Russell, Y. Li and D. Wang, Understanding the Morphology of High-Performance Solar Cells Based on a Low-Cost Polymer Donor, *ACS Appl. Mater. Interfaces*, 2020, **12**, 9537–9544, DOI: 10.1021/acsmi.9b22666.
- J. Yuan, Y. Zhang, L. Zhou, G. Zhang, H. Yip, T. Lau, X. Lu, C. Zhu, H. Peng, P. A. Johnson, M. Leclerc, Y. Cao, J. Ulanski, Y. Li and Y. Zou, Single-Junction Organic Solar Cell with over 15% Efficiency Using Fused-Ring Acceptor with Electron-Deficient Core Single-Junction, *Joule*, 2019, **3**, 1–12, DOI: 10.1016/j.joule.2019.01.004.
- T. Wang, J. Qin, Z. Xiao, X. Meng, C. Zuo, B. Yang, H. Tan, J. Yang, S. Yang, K. Sun, S. Xie and L. Ding, Short Communication A 2.16 eV Bandgap Polymer Donor Gives 16% Power Conversion Efficiency, *Sci. Bull.*, 2020, **65**(3), 179–181, DOI: 10.1016/j.scib.2019.11.030.
- C. J. Brabec, M. Heeney, I. McCulloch and J. Nelson, Influence of Blend Microstructure on Bulk Heterojunction Organic Photovoltaic Performance, *Chem. Soc. Rev.*, 2011, **40**, 1185–1199, DOI: 10.1039/c0cs00045k.
- C. J. Schaffer, C. M. Palumbiny, M. A. Niedermeier, C. Jendrzewski, G. Santoro, S. V. Roth and P. Müller-Buschbaum, A Direct Evidence of Morphological Degradation on a Nanometer Scale in Polymer Solar Cells, *Adv. Mater.*, 2013, **25**(46), 6760–6764, DOI: 10.1002/adma.201302854.
- Y. Zhang, Y. Xu, M. J. Ford, F. Li, J. Sun and X. Ling, Thermally Stable All-Polymer Solar Cells with High Tolerance on Blend Ratios, *Adv. Energy Mater.*, 2018, **8**(1800029), 1–10, DOI: 10.1002/aenm.201800029.
- A. L. Ayzner, C. J. Tassone, S. H. Tolbert and B. J. Schwartz, Reappraising the Need for Bulk Heterojunctions in Polymer - Fullerene Photovoltaics: The Role of Carrier Transport in All-Solution-Processed P3HT/PCBM Bilayer Solar Cells, *J. Phys. Chem. C*, 2009, **113**, 20050–20060, DOI: 10.1021/jp9050897.
- A. J. Clulow, C. Tao, K. H. Lee, M. Velusamy, J. A. Mcewan, P. E. Shaw, N. L. Yamada, M. James, P. L. Burn, I. R. Gentle and P. Meredith, Time-Resolved Neutron Reflectometry and Photovoltaic Device Studies on Sequentially Deposited PCDTBT-Fullerene Layers, *Langmuir*, 2014, **30**, 11474–11484, DOI: 10.1021/la5020779.
- B. Yang, Y. Yuan and J. Huang, Reduced Bimolecular Charge Recombination Loss in Thermally Annealed Bilayer Heterojunction Photovoltaic Devices with Large External Quantum Efficiency and Fill Factor, *J. Phys. Chem. C*, 2014, **118**, 5196–5202, DOI: 10.1021/jp500547j.



- 25 P. Cheng, C. Yan, Y. Wu, S. Dai, W. Ma and X. Zhan, Efficient and Stable Organic Solar Cells via Sequential Process, *J. Mater. Chem. C*, 2016, **4**(34), 8086–8093, DOI: 10.1039/C6TC02338J.
- 26 Y. Jang, Y. J. Cho, M. Kim, J. Seok, H. Ahn and K. Kim, Formation of Thermally Stable Bulk Heterojunction by Reducing the Polymer and Fullerene Intermixing, *Sci. Rep.*, 2017, **7**(9690), 1–9, DOI: 10.1038/s41598-017-09167-4.
- 27 M. T. Fontana, T. J. Aubry, D. T. Scholes, S. A. Hawks and B. J. Schwartz, Sequential Processing: A Rational Route for Bulk Heterojunction Formation via Polymer Swelling, in *Handbook of Organic*, 2018, vol. 4, pp. 1–40, DOI: 10.1142/9789813239517\_0008.
- 28 R. Sun, J. Guo, C. Sun, T. Wang, Z. Luo, Z. Zhang, X. Jiao, W. Tang, C. Yang, Y. Li and J. Min, A Universal Layer-by-Layer Solution-Processing Approach for Efficient Non-Fullerene Organic Solar, *Energy Environ. Sci.*, 2019, **12**, 384–395, DOI: 10.1039/c8ee02560f.
- 29 L. Arunagiri, G. Zhang, H. Hu, H. Yao, K. Zhang, Y. Li, P. C. Y. Chow, H. Ade and H. Yan, Temperature-Dependent Aggregation Donor Polymers Enable Highly Efficient Sequentially Processed Organic Photovoltaics Without the Need of Orthogonal Solvents, *Adv. Funct. Mater.*, 2019, **29**(1902478), 1–10, DOI: 10.1002/adfm.201902478.
- 30 S. Dong, K. Zhang, B. Xie, J. Xiao, H. Yip, H. Yan and F. Huang, High-Performance Large-Area Organic Solar Cells Enabled by Sequential Bilayer Processing via Non-halogenated Solvents, *Adv. Energy Mater.*, 2019, **9**(1802832), 1–7, DOI: 10.1002/aenm.201802832.
- 31 R. Sun, Q. Wu, J. Guo, T. Wang, Y. Wu, B. Qiu, Z. Luo, W. Yang, Z. Hu, J. Guo, M. Shi, C. Yang, F. Huang, Y. Li and J. Min, A Layer-by-Layer Architecture for Printable Organic Solar Cells Overcoming the Scaling Lag of Module Efficiency, *Joule*, 2020, **4**, 1–13, DOI: 10.1016/j.joule.2019.12.004.
- 32 S. Collavini and J. L. Delgado, Fullerenes: The Stars of Photovoltaics. *Sustain, Energy Fuels*, 2018, **2**, 2480–2493, DOI: 10.1039/c8se00254a.
- 33 R. C. Haddon, R. E. Palmer, H. W. Kroto and P. A. Sermon, The Fullerenes: Powerful Carbon-Based Electron Acceptors, *Philos. Trans. R. Soc., A*, 1993, **343**, 53–62, DOI: 10.1098/rsta.1993.0040.
- 34 B. H. Imahori and Y. Sakata, Donor-Linked Fullerenes: Photoinduced Electron Transfer and Its Potential Application\*\*, *Adv. Mater.*, 1997, **9**(7), 537–546, DOI: 10.1002/adma.19970090704.
- 35 N. Sivaraman, R. Dhamodaran, I. Kaliappan, T. G. Srinivasan, P. R. Vasudeva Rao and C. K. Mathews, Solubility of C60 in Organic Solvents, *J. Org. Chem.*, 1992, **57**, 6077–6079, DOI: 10.1021/jo00048a056.
- 36 G. Yu, J. Gao, C. J. Hummelen, F. Wudl and A. J. Heeger, Polymer Photovoltaic Cells: Enhanced Efficiencies via a Network of Internal Donor-Acceptor Heterojunctions, *Science*, 1995, **270**(5243), 1789–1792, DOI: 10.1126/science.270.5243.1789.
- 37 S. M. Mortuza, C. Cisneros, M. Bartolo and S. Banerjee, Molecular Modeling of Nanoparticles and Conjugated Polymers During Synthesis of Photoactive Layers of Organic Photovoltaic Solar Cells, *2013 AIChE Annual Meeting*, 2013.
- 38 W. J. Potscavage, S. Yoo, B. Domercq, J. Kim and B. Kippelen, Integrated Organic Photovoltaic Modules, *Proc. SPIE*, 2007, **6656**(66560R), 1–10, DOI: 10.1117/12.735320.
- 39 E. T. Hoke, K. Vandewal, J. A. Bartelt, W. R. Mateker, J. D. Douglas, R. Noriega, K. R. Graham, J. M. J. Fréchet, A. Salles and M. D. McGehee, Recombination in Polymer: Fullerene Solar Cells with Open-Circuit Voltages Approaching and Exceeding 1.0 V, *Adv. Energy Mater.*, 2013, **3**(2), 220–230, DOI: 10.1002/aenm.201200474.
- 40 H. Li and J. Wang, Layer-by-Layer Processed High-Performance Polymer Solar Cells, *Appl. Phys. Lett.*, 2012, **101**(263901), 1–5, DOI: 10.1063/1.4773515.
- 41 P. A. Troshin, S. I. Troyanov, G. N. Boiko, N. Rimma, A. N. Lapshin and N. F. Goldshleger, Efficient 2 + 3 Cycloaddition Approach to Synthesis of Pyridinyl Based [60] Fullerene Ligands Synthesis of Pyridinyl Based, *Fullerenes, Nanotubes, Carbon Nanostruct.*, 2004, **12**(1–2), 413–419, DOI: 10.1081/FST-120027200.
- 42 M. Egginger, R. Koeppel, F. Meghdadi, P. A. Troshin, R. N. Lyubovskaya, D. Meissner and N. S. Sariciftci, Comparative Studies on Solar Cell Structures Using Zinc Phthalocyanine, *Proc. SPIE*, 2006, **6192**(61921Y), 1–8, DOI: 10.1117/12.662909.
- 43 R. Koeppel, N. S. Sariciftci, P. A. Troshin and R. N. Lyubovskaya, Complexation of Pyrrolidinofullerenes and Zinc-Phthalocyanine in a Bilayer Organic Solar Cell Structure, *Appl. Phys. Lett.*, 2007, **87**(244102), 1–3, DOI: 10.1063/1.2146070.
- 44 Y. Zhang, M. T. Sajjad, O. Blaszczyk, A. Ruseckas, L. A. Serrano, G. Cooke and I. D. W. Samuel, Enhanced Exciton Harvesting in a Planar Heterojunction Organic Photovoltaic Device by Solvent Vapor Annealing, *Org. Electron.*, 2019, **70**, 162–166, DOI: 10.1016/j.orgel.2019.03.014.
- 45 Y. Wang, H. Benten, S. Ohara, D. Kawamura, H. Ohkita and S. Ito, Measurement of Exciton Diffusion in a Well-Defined Donor/Acceptor Heterojunction Based on a Conjugated Polymer and Cross-Linked Fullerene Derivative, *ACS Appl. Mater. Interfaces*, 2014, **6**, 14108–14115, DOI: 10.1021/am503434p.
- 46 C. Z. Li, H. L. Yip and A. K. Y. Jen, Functional Fullerenes for Organic Photovoltaics, *J. Mater. Chem.*, 2012, **22**(10), 4161–4177, DOI: 10.1039/c2jm15126j.
- 47 A. Polman, M. Knight, E. C. Garnett, B. Ehrler and W. C. Sinke, Photovoltaic Materials: Present Efficiencies and Future Challenges, *Science*, 2016, **352**(6283), 1–10, DOI: 10.1126/science.aad4424.
- 48 Y. Lin, J. Wang, Z. Zhang, H. Bai, Y. Li, D. Zhu and X. Zhan, An Electron Acceptor Challenging Fullerenes for Efficient Polymer Solar Cells, *Adv. Mater.*, 2015, **27**, 1170–1174, DOI: 10.1002/adma.201404317.
- 49 L. Huang, P. Jiang, Y. Zhang, L. Zhang, Z. Yu and Q. He, Unraveling the Morphology in Solution-Processed Pseudo-Bilayer Planar Heterojunction Organic Solar Cells, *ACS*



- Appl. Mater. Interfaces*, 2019, **11**, 26213–26221, DOI: 10.1021/acsami.9b10689.
- 50 Y. Lin, F. Zhao, Q. He, L. Huo, Y. Wu, T. C. Parker, W. Ma, Y. Sun, C. Wang, D. Zhu, A. J. Heeger, S. R. Marder and X. Zhan, High-Performance Electron Acceptor with Thienyl Side Chains for Organic Photovoltaics, *J. Am. Chem. Soc.*, 2016, **138**, 4955–4961, DOI: 10.1021/jacs.6b02004.
- 51 S. Li, L. Ye, W. Zhao, S. Zhang, S. Mukherjee, H. Ade and J. Hou, Energy-Level Modulation of Small-Molecule Electron Acceptors to Achieve over 12% Efficiency in Polymer Solar Cells, *Adv. Mater.*, 2016, **28**, 9423–9429, DOI: 10.1002/adma.201602776.
- 52 H. Yao, L. Ye, J. Hou, B. Jang, G. Han, Y. Cui, G. M. Su, C. Wang, B. Gao, R. Yu, H. Zhang, Y. Yi, H. Y. Woo, H. Ade and J. Hou, Achieving Highly Efficient Nonfullerene Organic Solar Cells with Improved Intermolecular Interaction and Open-Circuit Voltage, *Adv. Mater.*, 2017, **29**(1700254), 1–8, DOI: 10.1002/adma.201700254.
- 53 Z. Zhang, J. Yu, X. Yin, Z. Hu, Y. Jiang, J. Sun, J. Zhou, F. Zhang, T. P. Russell, F. Liu and W. Tang, Conformation Locking on Fused-Ring Electron Acceptor for High-Performance Nonfullerene Organic Solar Cells, *Adv. Funct. Mater.*, 2018, **28**(1705095), 1–8, DOI: 10.1002/adfm.201705095.
- 54 X. Li, J. Yao, I. Angunawela, C. Sun, L. Xue, A. Liebman-pelaez, C. Zhu, C. Yang, Z. Zhang, H. Ade and Y. Li, Improvement of Photovoltaic Performance of Polymer Solar Cells by Rational Molecular Optimization of Organic Molecule Acceptors, *Adv. Energy Mater.*, 2018, **8**(1800815), 1–7, DOI: 10.1002/aenm.201800815.
- 55 Y. Zhang, H. Yao, S. Zhang, Y. Qin, J. Zhang, L. Yang, W. Li, Z. Wei, F. Gao and J. Hou, Fluorination vs. Chlorination: A Case Study on High Performance Organic Photovoltaic Materials, *Sci. China: Chem.*, 2018, **61**(10), 1328–1337, DOI: 10.1007/s11426-018-9260-2.
- 56 B. Kan, J. Zhang, F. Liu, X. Wan, C. Li, X. Ke, Y. Wang, H. Feng, Y. Zhang, G. Long, R. H. Friend, A. A. Bakulin and Y. Chen, Fine-Tuning the Energy Levels of a Nonfullerene Small-Molecule Acceptor to Achieve a High Short-Circuit Current and a Power Conversion Efficiency over 12% in Organic Solar Cells, *Adv. Energy Mater.*, 2018, **30**(1704904), 1–8, DOI: 10.1002/adma.201704904.
- 57 Y. Lin, Q. He, F. Zhao, L. Huo, J. Mai, X. Lu, C. Su, T. Li, J. Wang, J. Zhu, Y. Sun, C. Wang and X. Zhan, A Facile Planar Fused-Ring Electron Acceptor for As-Cast Polymer Solar Cells with 8.71% Efficiency, *J. Am. Chem. Soc.*, 2016, **138**, 2973–2976, DOI: 10.1021/jacs.6b00853.
- 58 H. Li, Y. Zhao, J. Fang, X. Zhu, B. Xia, K. Lu, Z. Wang, J. Zhang, X. Guo and Z. Wei, Improve the Performance of the All-Small-Molecule Nonfullerene Organic Solar Cells through Enhancing the Crystallinity of Acceptors, *Adv. Energy Mater.*, 2018, **8**(1702377), 1–8, DOI: 10.1002/aenm.201702377.
- 59 Y. Cui, S. Zhang, N. Liang, J. Kong, C. Yang and H. Yao, Toward Efficient Polymer Solar Cells Processed by a Solution-Processed Layer-By-Layer Approach, *Adv. Mater.*, 2018, **30**(1802499), 1–7, DOI: 10.1002/adma.201802499.
- 60 Y. Cui, H. Yao, J. Zhang, T. Zhang, Y. Wang, L. Hong, K. Xian, B. Xu, S. Zhang, J. Peng, Z. Wei, F. Gao and J. Hou, Over 16% Efficiency Organic Photovoltaic Cells Enabled by a Chlorinated Acceptor with Increased Open-Circuit Voltages, *Nat. Commun.*, 2019, **10**(2515), 1–8, DOI: 10.1038/s41467-019-10351-5.
- 61 Z. Luo, X. Jiao, J. Min and C. Yang, Altering Alkyl-Chains Branching Positions for Boosting the Performance of Small-Molecule Acceptors for Highly Efficient Nonfullerene Organic Solar Cells, *Sci. China: Chem.*, 2020, **63**(3), 361–369, DOI: 10.1007/s11426-019-9670-2.
- 62 M. T. Lloyd, A. C. Mayer, A. S. Tayi, A. M. Bowen, T. G. Kasen, D. J. Herman, D. A. Mourey, J. E. Anthony and G. G. Malliaras, Photovoltaic Cells from a Soluble Pentacene Derivative, *Org. Electron.*, 2006, **7**, 243–248, DOI: 10.1016/j.orgel.2006.03.002.
- 63 A. A. Gorodetsky, M. Cox, N. J. Tremblay, I. Kyymissis and C. Nuckolls, Solar Cells from a Solution Processable Pentacene with Improved Air Stability, *Chem. Mater.*, 2009, **21**, 4090–4092, DOI: 10.1021/cm9016134.
- 64 S. Sreejith, P. Carol, P. Chithra and A. Ajayaghosh, Squaraine Dyes: A Mine of Molecular Materials, *J. Mater. Chem.*, 2008, **18**, 264–274, DOI: 10.1039/b707734c.
- 65 G. Chen, H. Sasabe, T. Igarashi, Z. Hong and J. Kido, Squaraine Dyes for Organic Photovoltaic Cells, *J. Mater. Chem. A*, 2015, **3**, 14517–14534, DOI: 10.1039/c5ta01879j.
- 66 G. Wei, X. Xiao, S. Wang, K. Sun, K. J. Bergemann, M. E. Thompson and S. R. Forrest, Functionalized Squaraine Donors for Nanocrystalline Organic Photovoltaics, *ACS Nano*, 2012, **6**(1), 972–978, DOI: 10.1021/nn204676j.
- 67 Q. Liu, S. E. Bottle and P. Sonar, Developments of Diketopyrrolopyrrole-Dye-Based Organic Semiconductors for a Wide Range of Applications in Electronics, *Adv. Mater.*, 2020, **32**(1903882), 1–46, DOI: 10.1002/adma.201903882.
- 68 W. Kylberg, P. Sonar, J. Heier, J. Tisserant, C. Müller, F. Nüesch, Z. Chen, A. Dodabalapur, S. Yoon and R. Hany, Synthesis, Thin-Film Morphology, and Comparative Study of Bulk and Bilayer Heterojunction Organic Photovoltaic Devices Using Soluble Diketopyrrolopyrrole Molecules, *Energy Environ. Sci.*, 2011, **4**, 3617–3624, DOI: 10.1039/c1ee01544c.
- 69 Y. Liu, X. Wan, F. Wang, J. Zhou, G. Long, J. Tian and Y. Chen, High-Performance Solar Cells Using a Solution-Processed Small Molecule Containing Benzodithiophene Unit, *Adv. Mater.*, 2011, **23**, 5387–5391, DOI: 10.1002/adma.201102790.
- 70 J. Zhou, Y. Zuo, X. Wan, G. Long, Q. Zhang, W. Ni, Y. Liu, Z. Li, G. He, C. Li, B. Kan, M. Li and Y. Chen, Solution-Processed and High-Performance Organic Solar Cells Using Small Molecules with a Benzodithiophene Unit, *J. Am. Chem. Soc.*, 2013, **135**, 8484–8487, DOI: 10.1021/ja403318y.
- 71 Y. Lin, L. Ma, Y. Li, Y. Liu, D. Zhu and X. Zhan, Small-Molecule Solar Cells with Fill Factors up to 0.75 via a Layer-by-Layer Solution Process, *Adv. Energy Mater.*, 2014, **4**(1300626), 1–6, DOI: 10.1002/aenm.201300626.
- 72 F. Meng, K. Chen, H. Tian, L. Zuppiroli and F. Nüesch, Cyanine Dye Acting Both as Donor and Acceptor in



- Heterojunction Photovoltaic Devices, *Appl. Phys. Lett.*, 2003, **82**(21), 3788–3790, DOI: 10.1063/1.1579133.
- 73 F. Nüesch, A. Faes, L. Zuppiroli, F. Meng, K. Chen and H. Tian, Counterion Effects in Cyanine Heterojunction Photovoltaic Devices, *J. Mater. Sci.*, 2005, **40**, 1353–1357, DOI: 10.1007/s10853-005-0564-4.
- 74 B. Fan, R. Hany, J.-E. Moser and F. Nüesch, Enhanced Cyanine Solar Cell Performance upon Oxygen Doping, *Org. Electron.*, 2008, **9**, 85–94, DOI: 10.1016/j.orgel.2007.09.008.
- 75 R. Hany, B. Fan, F. A. Castro, J. de Heier, W. Kylberg and F. Nüesch, Strategies to Improve Cyanine Dye Multi Layer Organic Solar Cells, *Prog. Photovoltaics*, 2011, **19**, 851–857, DOI: 10.1002/pip.
- 76 F. A. Castro, A. Faes, T. Geiger, C. F. O. Graeff, M. Nagel, F. Nüesch and R. Hany, On the Use of Cyanine Dyes as Low-Bandgap Materials in Bulk Heterojunction Photovoltaic Devices, *Synth. Met.*, 2006, **156**, 973–978, DOI: 10.1016/j.synthmet.2006.06.010.
- 77 H. Zhang, G. Wicht, C. Gretener, M. Nagel, F. Nüesch, Y. Romanyuk, J. Tisserant and R. Hany, Semitransparent Organic Photovoltaics Using a Near-Infrared Absorbing Cyanine Dye, *Sol. Energy Mater. Sol. Cells*, 2013, **118**, 157–164, DOI: 10.1016/j.solmat.2013.08.011.
- 78 O. Malinkiewicz, T. Grancha, A. Molina-Ontoria, A. Soriano, H. Brine and H. J. Bolink, Efficient, Cyanine Dye Based Bilayer Solar Cells, *Adv. Energy Mater.*, 2013, **3**, 472–477, DOI: 10.1002/aenm.201200764.
- 79 L. Wang, C. Hinderling, S. Jenatsch, F. Nüesch, D. Rentsch, R. Steim, H. Zhang and R. Hany, Cyanine Dye Polyelectrolytes for Organic Bilayer Solar Cells, *Polymer*, 2014, **55**, 3195–3201, DOI: 10.1016/j.polymer.2014.05.035.
- 80 A. Mahmood, J.-Y. Hu, B. Xiao, A. Tang, X. Wang and E. Zhou, Recent Progress in Porphyrin-Based Materials for Organic Solar Cells, *J. Mater. Chem. A*, 2018, **6**, 16769–16797, DOI: 10.1039/c8ta06392c.
- 81 R. R. Zope, M. Olguin and T. Baruah, Charge Transfer Excitations in Cofacial Fullerene-Porphyrin Complexes, *J. Chem. Phys.*, 2012, **137**(084317), 1–8, DOI: 10.1063/1.4739272.
- 82 Y. Sato, T. Niinomi, M. Hashiguchi, Y. Matsuo and E. Nakamura, Organic Photovoltaic Based on Solution-Processed Benzoporphyrin, *Proc. SPIE*, 2007, **6656**(66560U), 1–9, DOI: 10.1117/12.733804.
- 83 Q. Sun, L. Dai, X. Zhou, L. Li and Q. Li, Bilayer- and Bulk-Heterojunction Solar Cells Using Liquid Crystalline Porphyrins as Donors by Solution Processing, *Appl. Phys. Lett.*, 2007, **91**(253505), 1–3, DOI: 10.1063/1.2823586.
- 84 B. M. D. Perez, C. Borek, P. I. Djurovich, E. I. Mayo, R. R. Lunt, S. R. Forrest and M. E. Thompson, Organic Photovoltaics Using Tetraphenylbenzoporphyrin Complexes as Donor Layers, *Adv. Mater.*, 2009, **21**, 1517–1520, DOI: 10.1002/adma.200802683.
- 85 A. Huijser, T. J. Savenije, A. Shalav and L. D. A. Siebbeles, An Experimental Study on the Molecular Organization and Exciton Diffusion in a Bilayer of a Porphyrin and Poly(3-Hexylthiophene), *J. Appl. Phys.*, 2008, **104**(034505), 1–10, DOI: 10.1063/1.2958325.
- 86 F. Ghani, I. Bochukov, K. Fostiropoulos and H. Riegler, Hybrid Solution/Vacuum-Processed Bilayer Heterojunction Organic Solar Cells: Structural Characterization and Performance, *Thin Solid Films*, 2012, **525**, 177–181, DOI: 10.1016/j.tsf.2012.10.045.
- 87 S. Schumann, R. A. Hatton and T. S. Jones, Organic Photovoltaic Devices Based on Water-Soluble Copper Phthalocyanine, *J. Phys. Chem. C*, 2011, **115**, 4916–4921, DOI: 10.1021/jp109544m.
- 88 M. D. M. Faure, T. M. Grant and B. H. Lessard, Silicon Phthalocyanines as Acceptor Candidates in Mixed Solution/Evaporation Processed Planar Heterojunction Organic Photovoltaic Devices, *Coatings*, 2019, **9**(203), 1–13, DOI: 10.3390/coatings9030203.
- 89 D. S. Josey, J. S. Castrucci, J. D. Dang, B. H. Lessard and T. P. Bender, Evaluating Thiophene Electron-Donor Layers for the Rapid Assessment of Boron Subphthalocyanines as Electron Acceptors in Organic Photovoltaics: Solution or Vacuum Deposition?, *ChemPhysChem*, 2015, **16**(6), 1245–1250, DOI: 10.1002/cphc.201402751.
- 90 C. G. Claessens, D. Gonzalez-Rodriguez and T. Torres, Subphthalocyanines: Singular Nonplanar Aromatic Compounds-Synthesis, Reactivity, and Physical Properties, *Chem. Rev.*, 2002, **102**(3), 835–853, DOI: 10.1021/cr0101454.
- 91 M. Jean, B. Ma, Y. Miyamoto, C. H. Woo and J. M. J. Fréchet, Solution Processable Boron Subphthalocyanine Derivatives as Active Materials for Organic Photovoltaics, *Proc. SPIE*, 2009, **7416**(74161E), 1–6, DOI: 10.1117/12.825372.
- 92 C. E. Mauldin, C. Piliago, D. Poulsen, D. A. Unruh, C. Woo, B. Ma, J. L. Mynar and J. M. J. Fréchet, Axial Thiophene-Boron(Subphthalocyanine) Dyads and Their Application in Organic Photovoltaics, *ACS Appl. Mater. Interfaces*, 2010, **2**(10), 2833–2838, DOI: 10.1021/am100516a.
- 93 B. Ma, C. H. Woo, Y. Miyamoto and J. M. J. Fréchet, Solution Processing of a Small Molecule, Subnaphthalocyanine, for Efficient Organic Photovoltaic Cells, *Chem. Mater.*, 2009, **21**, 1413–1417, DOI: 10.1021/cm900005g.
- 94 S. Y. Leblebici, L. Catane, D. E. Barclay, T. Olson, T. L. Chen and B. Ma, Near-Infrared Azadipyromethenes as Electron Donor for Efficient Planar Heterojunction Organic Solar Cells, *ACS Appl. Mater. Interfaces*, 2011, **3**, 4469–4474, DOI: 10.1021/am201157d.
- 95 N. S. Sariciftci, L. Smilowitz, A. J. Heeger and F. Wudl, Semiconducting Polymers (as Donors) and Buckminsterfullerene (as Acceptor): Photoinduced Electron Transfer and Heterojunction Devices, *Synth. Met.*, 1993, **59**, 333–352, DOI: 10.1016/0379-6779(93)91166-Y.
- 96 N. S. Sariciftci, D. Braun, C. Zhang, V. I. Srdanov, A. J. Heeger, G. Stucky and F. Wudl, Semiconducting Polymer-Buckminsterfullerene Heterojunctions: Diodes, Photodiodes, and Photovoltaic Cells, *Appl. Phys. Lett.*, 1993, **62**(6), 585–587, DOI: 10.1063/1.108863.
- 97 D. Vacar, E. S. Maniloff, D. W. Mcbranch and A. J. Heeger, Charge-Transfer Range for Photoexcitation in Conjugated Polymer/Fullerene Bilayers and Blends, *Phys. Rev. B: Condens. Matter Mater. Phys.*, 1997, **56**(8), 4573–4577, DOI: 10.1103/PhysRevB.56.4573.



- 98 J. J. M. Halls, K. Pichler, R. H. Friend, S. C. Moratti and A. B. Holmes, Exciton Diffusion and Dissociation in a Poly-(p-Phenylenevinylene)/C60 Heterojunction Photovoltaic Cell, *Appl. Phys. Lett.*, 1996, **68**(22), 3120–3122.
- 99 T. Stübinger and W. Brütting, Exciton Diffusion and Optical Interference in Organic Donor – Acceptor Photovoltaic Cells, *J. Appl. Phys.*, 2001, **90**(7), 3632–3641, DOI: 10.1063/1.1394920.
- 100 M. Drees, K. Premaratne, W. Graupner, J. R. Heflin, R. M. Davis, D. Marciu and M. Miller, Creation of a Gradient Polymer-Fullerene Interface in Photovoltaic Devices by Thermally Controlled Interdiffusion, *Appl. Phys. Lett.*, 2002, **81**(24), 4607–4609, DOI: 10.1063/1.1522830.
- 101 M. Drees, R. M. Davis and J. R. Heflin, Thickness Dependence, in Situ Measurements, and Morphology of Thermally Controlled Interdiffusion in Polymer-C60 Photovoltaic Devices, *Phys. Rev. B: Condens. Matter Mater. Phys.*, 2004, **69**(165320), 1–6, DOI: 10.1103/PhysRevB.69.165320.
- 102 L. Chen, D. Godovsky, O. Inganäs, J. C. Hummelen, R. A. J. Janssens, M. Svensson and M. R. Anderson, Polymer Photovoltaic Devices from Stratified Multilayers of Donor-Acceptor Blends, *Adv. Mater.*, 2000, **12**(18), 1367–1370, DOI: 10.1002/1521-4095(200009)12:18:3.CO;2-Z.
- 103 B. A. Collins, E. Gann, L. Guignard, X. He, C. R. McNeill and H. Ade, Molecular Miscibility of Polymer - Fullerene Blends, *J. Phys. Chem. Lett.*, 2010, **1**, 3160–3166, DOI: 10.1021/jz101276h.
- 104 C. Schlebusch, B. Kessler, S. Cramm and W. Eberhardt, Organic Photoconductors and C60, *Synth. Met.*, 1996, **77**, 151–154, DOI: 10.1016/0379-6779(96)80077-4.
- 105 A. Gopal, M. Drees, R. M. Davis and J. R. Heflin, Modelling of External Quantum Efficiency Spectra as a Function of Varying P3OT Thickness in P3OT-C60 Polymer Photovoltaic Devices, *Proc. SPIE*, 2005, **5938**(593813), 1–10, DOI: 10.1117/12.615987.
- 106 M. Drees, R. M. Davis and J. R. Heflin, Improved Morphology of Polymer-Fullerene Photovoltaic Devices with Thermally Induced Concentration Gradients, *J. Appl. Phys.*, 2005, **97**(036103), 1–3, DOI: 10.1063/1.1845574.
- 107 K. Kim, J. Liu and D. L. Carroll, Thermal Diffusion Processes in Bulk Heterojunction Formation for Poly-3- Hexylthiophene/Single Heterojunction Photovoltaics, *Appl. Phys. Lett.*, 2006, **88**(181911), 1–3, DOI: 10.1063/1.2199970.
- 108 D. Yu, Y. Yang, M. Durstock, J. Baek and L. Dai, Soluble P3HT-Grafted Graphene for Efficient Bilayer-Heterojunction Photovoltaic Devices, *ACS Nano*, 2010, **4**(10), 5633–5640, DOI: 10.1021/nn101671t.
- 109 L. Tan, M. D. Curtis and A. H. Francis, Charge Transfer in Ferrocene-Bearing Poly(Thiophene)s and Application in Organic Bilayer Photocells, *Macromolecules*, 2002, **35**, 4628–4635, DOI: 10.1021/ma012183v.
- 110 D. M. Stevens, Y. Qin, M. A. Hillmyer and C. D. Frisbie, Enhancement of the Morphology and Open Circuit Voltage in Bilayer Polymer/Fullerene Solar Cells, *J. Phys. Chem. C*, 2009, **113**, 11408–11415, DOI: 10.1021/jp902198y.
- 111 A. S. Ferreira, J. C. Aguirre, S. Subramanian, S. A. Jenekhe, S. H. Tolbert and B. J. Schwartz, Understanding How Polymer Properties Control OPV Device Performance: Regioregularity, Swelling, and Morphology Optimization Using Random Poly(3-Butylthiophene-Co-3-Octylthiophene) Polymers, *J. Phys. Chem. C*, 2016, **120**, 22115–22125, DOI: 10.1021/acs.jpcc.6b03300.
- 112 D. Kekuda, J. Huang, K. Ho and C. Chu, Modulation of Donor - Acceptor Interface through Thermal Treatment for Efficient Bilayer Organic Solar Cells, *J. Phys. Chem. C*, 2010, **114**, 2764–2768, DOI: 10.1021/jp910023d.
- 113 J. Seok, T. J. Shin, S. Park, C. Cho, J. Y. Lee, D. Y. Ryu, M. H. Kim and K. Kim, Efficient Organic Photovoltaics Utilizing Nanoscale Heterojunctions in Sequentially Deposited Polymer/Fullerene Bilayer, *Sci. Rep.*, 2015, **5**(8373), 1–9, DOI: 10.1038/srep08373.
- 114 Y. Tang, H. Sun, Z. Wu, Y. Zhang, G. Zhang, M. Su, X. Zhou, X. Wu, W. Sun, X. Zhang, B. Liu, W. Chen, Q. Liao, H. Y. Woo and X. Guo, A New Wide Bandgap Donor Polymer for Efficient Nonfullerene Organic Solar Cells with a Large Open-Circuit Voltage, *Adv. Sci.*, 2019, **6**(1901773), 1–10, DOI: 10.1002/advs.201901773.
- 115 M. Zhang, X. Guo, W. Ma, H. Ade and J. Hou, A Polythiophene Derivative with Superior Properties for Practical Application in Polymer Solar Cells, *Adv. Mater.*, 2014, **26**, 5880–5885, DOI: 10.1002/adma.201401494.
- 116 B. Zheng, L. Huo and Y. Li, Benzodithiophenedione-Based Polymers: Recent Advances in Organic Photovoltaics, *NPG Asia Mater.*, 2020, **12**(3), 1–22, DOI: 10.1038/s41427-019-0163-5.
- 117 C. Sun, F. Pan, H. Bin, J. Zhang, L. Xue, B. Qiu, Z. Wei, Z. Zhang and Y. Li, A Low Cost and High Performance Polymer Donor Material for Polymer Solar Cells, *Nat. Commun.*, 2018, **9**(743), 1–10, DOI: 10.1038/s41467-018-03207-x.
- 118 H. Bin, Z. Zhang, L. Gao, S. Chen, L. Zhong, L. Xue, C. Yang and Y. Li, Non-Fullerene Polymer Solar Cells Based on Alkylthio and Fluorine Substituted 2D-Conjugated Polymers Reach 9.5% Efficiency, *J. Am. Chem. Soc.*, 2016, **138**, 4657–4664, DOI: 10.1021/jacs.6b01744.
- 119 H. Bin, L. Gao, Z. Zhang, Y. Yang, Y. Zhang, C. Zhang, S. Chen, L. Xue, C. Yang, M. Xiao and Y. Li, 11.4% Efficiency Non-Fullerene Polymer Solar Cells with Trialkylsilyl Substituted 2D-Conjugated Polymer as Donor, *Nat. Commun.*, 2016, **7**(13651), 1–11, DOI: 10.1038/ncomms13651.
- 120 Z. Li, K. Jiang, G. Yang, J. Yuk, L. Lai, T. Ma, J. Zhao, W. Ma and H. Yan, Donor Polymer Design Enables Efficient Non-Fullerene Organic Solar Cells, *Nat. Commun.*, 2016, **7**(13094), 1–9, DOI: 10.1038/ncomms13094.
- 121 B. H. Smith, Q. Zhang, M. A. Kelly, J. H. Litofsky, D. Kumar, A. Hexemer, W. You and E. D. Gomez, Fluorination of Donor–Acceptor Copolymer Active Layers Enhances Charge Mobilities in Thin-Film Transistors, *ACS Macro Lett.*, 2017, **6**, 1162–1167, DOI: 10.1021/acsmacrolett.7b00716.
- 122 N. Zhou and A. Facchetti, Naphthalenediimide (NDI) Polymers for All-Polymer Photovoltaics, *Mater. Today*, 2018, **21**(4), 377–390, DOI: 10.1016/j.mattod.2018.02.003.
- 123 S. A. Jenekhe and S. Yi, Efficient Photovoltaic Cells from Semiconducting Polymer Heterojunctions, *Appl. Phys. Lett.*, 2000, **77**(17), 2635–2637, DOI: 10.1063/1.1320022.



- 124 S. Brixi, O. A. Melville, B. Mirka, Y. He, A. D. Hendsbee, H. Meng, Y. Li and B. H. Lessard, Air and Temperature Sensitivity of N-Type Polymer Materials to Meet and Exceed the Standard of N2200, *Sci. Rep.*, 2020, **10**(4014), 1–10, DOI: 10.1038/s41598-020-60812-x.
- 125 Y. Xu, J. Yuan, S. Liang, J. Chen, Y. Xia, B. W. Larson, Y. Wang, G. M. Su, Y. Zhang, C. Cui, M. Wang, H. Zhao and W. Ma, Simultaneously Improved Efficiency and Stability in All-Polymer Solar Cells by a P-i-N Architecture, *ACS Energy Lett.*, 2019, **4**, 2277–2286, DOI: 10.1021/acsenerylett.9b01459.
- 126 Y. Fang, H. Jin, A. Raynor, X. Wang, P. E. Shaw, N. Kopidakis, C. R. Mcneill and P. L. Burn, Application of an A–A′–A–Containing Acceptor Polymer in Sequentially Deposited All-Polymer Solar Cells, *ACS Appl. Mater. Interfaces*, 2018, **10**, 24046–24054, DOI: 10.1021/acsam.8b05875.
- 127 Z. Zhang, C. Zhan, X. Zhang, S. Zhang, J. Huang, A. D. Q. Li and J. Yao, A Self-Assembly Phase Diagram from Amphiphilic Perylene Diimides, *Chem. – Eur. J.*, 2012, **18**, 12305–12313, DOI: 10.1002/chem.201201352.
- 128 X. Zhan, Z. Tan, B. Domercq, Z. An, X. Zhang, S. Barlow, Y. Li, D. Zhu, B. Kippelen and S. R. Marder, A High-Mobility Electron-Transport Polymer with Broad Absorption and Its Use in Field-Effect Transistors and All-Polymer Solar Cells, *J. Am. Chem. Soc.*, 2007, **129**, 7246–7247, DOI: 10.1021/ja071760d.
- 129 Y. Wang, X. Zhao and X. Zhan, Layer by Layer Solution Processed Organic Solar Cells Based on a Small Molecule Donor and Acceptor, *J. Mater. Chem. C*, 2015, **3**, 447–452, DOI: 10.1039/c4tc02103g.
- 130 T. Shan, Y. Hong, L. Zhu, X. Wang, Y. Zhang, K. Ding, F. Liu, C. Chen and H. Zhong, Achieving Optimal Bulk Heterojunction in All-Polymer Solar Cells by Sequential Processing with Nonorthogonal Solvents, *ACS Appl. Mater. Interfaces*, 2019, **11**, 42438–42446, DOI: 10.1021/acsam.9b15476.
- 131 H. Zhong, C. Wu, C. Li, J. Carpenter, C. Chueh, J. Chen, H. Ade and A. K. Jen, Rigidifying Nonplanar Perylene Diimides by Ring Fusion Toward Geometry-Tunable Acceptors for High-Performance Fullerene-Free Solar Cells, *Adv. Mater.*, 2016, **28**, 951–958, DOI: 10.1002/adma.201504120.
- 132 B. H. Yan, S. Swaraj, C. Wang, I. Hwang, N. C. Greenham, C. Groves, H. Ade and C. R. Mcneill, Influence of Annealing and Interfacial Roughness on the Performance of Bilayer Donor/Acceptor Polymer Photovoltaic Devices, *Adv. Funct. Mater.*, 2010, **20**, 4329–4337, DOI: 10.1002/adfm.201001292.
- 133 K. Yao, J. J. Intemann, H. Yip, P. Liang and C. Chang, Efficient All Polymer Solar Cells from Layer-Evolved Processing of a Bilayer Inverted Structure, *J. Phys. Chem. C*, 2014, **2**, 416–420, DOI: 10.1039/c3tc31945h.
- 134 M. Kaur, A. Gopal, R. M. Davis and J. R. Hefflin, Concentration Gradient P3OT/PCBM Photovoltaic Devices Fabricated by Thermal Interdiffusion of Separately Spin-Cast Organic Layers, *Sol. Energy Mater. Sol. Cells*, 2009, **93**, 1779–1784, DOI: 10.1016/j.solmat.2009.06.009.
- 135 D. H. Wang, H. K. Lee, D.-G. Choi, J. H. Park and O. O. Park, Solution-Processable Polymer Solar Cells from a Poly(3-Hexylthiophene)/[6,6]-PhenylC61-Butyric Acidmethyl Ester Concentration Graded Bilayers, *Appl. Phys. Lett.*, 2009, **95**(043505), 1–3, DOI: 10.1063/1.3192360.
- 136 J. S. Moon, C. J. Takacs, Y. Sun and A. J. Heeger, Spontaneous Formation of Bulk Heterojunction Nanostructures: Multiple Routes to Equivalent Morphologies, *Nano Lett.*, 2011, **11**, 1036–1039, DOI: 10.1021/nl200056p.
- 137 D. H. Wang, J. K. Kim, O. O. Park and J. H. Park, Analysis of Surface Morphological Changes in Organic Photovoltaic Devices: Bilayer versus Bulk-Heterojunction, *Energy Environ. Sci.*, 2011, **4**, 1434–1439, DOI: 10.1039/c0ee00643b.
- 138 R. Zhu, A. Kumar and Y. Yang, Polarizing Organic Photovoltaics, *Adv. Mater.*, 2011, **23**, 4193–4198, DOI: 10.1002/adma.201101514.
- 139 K. H. Lee, P. E. Schwenn, A. R. G. Smith, H. Cavaye, P. E. Shaw, M. James, K. B. Krueger, I. R. Gentle, P. Meredith and P. L. Burn, Morphology of All-Solution-Processed “Bilayer” Organic Solar Cells, *Adv. Mater.*, 2011, **23**, 766–770, DOI: 10.1002/adma.201003545.
- 140 C. W. Rochester, S. A. Mauger and A. J. Moule, Investigating the Morphology of Polymer/Fullerene Layers Coated Using Orthogonal Solvents, *J. Phys. Chem. C*, 2012, **116**, 7287–7292, DOI: 10.1021/jp212341a.
- 141 A. Loiudice, A. Rizzo, M. Biasiucci and G. Gigli, Bulk Heterojunction versus Diffused Bilayer: The Role of Device Geometry in Solution p-Doped Polymer-Based Solar Cells, *J. Phys. Chem. Lett.*, 2012, **3**, 1908–1915, DOI: 10.1021/jz300754p.
- 142 V. Vohra, M. Campoy-Quiles, M. Garriga and H. Murata, Organic Solar Cells Based on Nanoporous P3HT Obtained from Self-Assembled P3HT:PS Templates, *J. Mater. Chem.*, 2012, **22**, 20017–20025, DOI: 10.1039/c2jm32639f.
- 143 V. Vohra, K. Higashimine, T. Murakami and H. Murata, Addition of Regiorandom Poly(3-Hexylthiophene) to Solution Processed Poly(3-Hexylthiophene):[6,6]-Phenyl-C61-Butyric Acid Methyl Ester Graded Bilayers to Tune the Vertical Concentration Gradient, *Appl. Phys. Lett.*, 2012, **101**(173301), 1–4, DOI: 10.1063/1.4761998.
- 144 A. Gadisa, J. R. Tumbleston, D. Ko, M. Aryal, R. Lopez and E. T. Samulski, The Role of Solvent and Morphology on Miscibility of Methanofullerene and Poly(3-Hexylthiophene), *Thin Solid Films*, 2012, **520**(16), 5466–5471, DOI: 10.1016/j.tsf.2012.03.117.
- 145 A. Loiudice, A. Rizzo, G. Latini, C. Nobile, M. De Giorgi and G. Gigli, Graded Vertical Phase Separation of Donor/Acceptor Species for Polymer Solar Cells, *Sol. Energy Mater. Sol. Cells*, 2012, **100**, 147–152, DOI: 10.1016/j.solmat.2012.01.006.
- 146 S.-M. Cho, J. Bae, E. Jang, M. Kim, C. Lee and S.-D. Lee, Solvent Effect of the Fibrillar Morphology on the Power Conversion Efficiency of a Polymer Photovoltaic Cell in a Diffusive Heterojunction, *Semicond. Sci. Technol.*, 2012, **27**(125018), 1–7, DOI: 10.1088/0268-1242/27/12/125018.
- 147 V. Vohra, G. Arrighetti, L. Barba, K. Higashimine, W. Porzio and H. Murata, Enhanced Vertical Concentration Gradient in Rubbed P3HT:PCBM Graded Bilayer Solar Cells, *J. Phys. Chem. Lett.*, 2012, **3**, 1820–1823, DOI: 10.1021/jz300710a.





- 148 H. Yeon, N. Su, J. Hong, Y. Song and T. Whan, Efficient Bilayer Heterojunction Polymer Solar Cells with Bumpy Donor – Acceptor Interface Formed by Facile Polymer Blend, *Org. Electron.*, 2012, **13**, 2688–2695, DOI: 10.1016/j.orgel.2012.07.040.
- 149 H. J. Park, J. Y. Lee, T. Lee and L. J. Guo, Advanced Heterojunction Structure of Polymer Photovoltaic Cell Generating High Photocurrent with Internal Quantum Efficiency Approaching 100%, *Adv. Energy Mater.*, 2013, **3**, 1135–1142, DOI: 10.1002/aenm.201300245.
- 150 M. K. Wong and K. Y. Wong, Investigation of the Factors Affecting the Power Conversion Efficiency of All-Solution-Processed ‘Bilayer’ P3HT:PCBM Solar Cells, *Synth. Met.*, 2013, **170**, 1–6, DOI: 10.1016/j.synthmet.2013.02.021.
- 151 H. Chen, S. Hu, H. Zang, B. Hu and M. Dadmun, Precise Structural Development and Its Correlation to Function in Conjugated Polymer: Fullerene Thin Films by Controlled Solvent Annealing, *Adv. Funct. Mater.*, 2013, **23**, 1701–1710, DOI: 10.1002/adfm.201202035.
- 152 H. Li, Z. Qi and J. Wang, Layer-by-Layer Processed Polymer Solar Cells with Self-Assembled Electron Buffer Layer, *Appl. Phys. Lett.*, 2013, **102**(213901), 1–5, DOI: 10.1063/1.4808047.
- 153 C. Tao, M. Aljada, P. E. Shaw, K. H. Lee, H. Cavaye, M. N. Balfour, R. J. Borthwick, M. James, P. L. Burn, I. R. Gentle and P. Meredith, Controlling Hierarchy in Solution-Processed Polymer Solar Cells Based on Crosslinked P3HT, *Adv. Energy Mater.*, 2013, **3**, 105–112, DOI: 10.1002/aenm.201200394.
- 154 K. H. Lee, Y. Zhang, P. L. Burn, I. R. Gentle, M. James, A. Nelson and P. Meredith, Correlation of Diffusion and Performance in Sequentially Processed P3HT/PCBM Heterojunction Films by Time-Resolved Neutron Reflectometry, *J. Phys. Chem. C*, 2013, **117**, 2593–2598, DOI: 10.1039/c3tc00063j.
- 155 P. Cheng, J. Hou, Y. Li and X. Zhan, Layer-by-Layer Solution-Processed Low-Bandgap Polymer-PC61BM Solar Cells with High Efficiency, *Adv. Energy Mater.*, 2014, **4**(1301349), 1–7, DOI: 10.1002/aenm.201301349.
- 156 S. A. Hawks, J. C. Aguirre, L. T. Schelhas, R. J. Thompson, R. C. Huber, A. S. Ferreira, G. Zhang, A. A. Herzing, S. H. Tolbert and B. J. Schwartz, Comparing Matched Polymer: Fullerene Solar Cells Made by Solution- Sequential Processing and Traditional Blend Casting: Nanoscale Structure and Device Performance, *J. Phys. Chem. C*, 2014, **118**, 17413–17425, DOI: 10.1021/jp504560r.
- 157 K. D. Kim, S. Park, S. Nho, G. Baek and S. Cho, The Effects of P3HT Crystallinity in Bilayer Structure Organic Solar Cells, *Curr. Appl. Phys.*, 2014, **14**, 1369–1373, DOI: 10.1016/j.cap.2014.07.019.
- 158 V. Vohra, K. Higashimine, S. Tsuzaki, K. Ohdaira and H. Murata, Formation of Vertical Concentration Gradients in Poly(3hexylthiophene-2,5diyl): Phenyl-C61-Butyric Acid Methyl Ester-Graded Bilayer Solar Cells, *Thin Solid Films*, 2014, **554**, 41–45, DOI: 10.1016/j.tsf.2013.05.171.
- 159 G. Zhang, R. C. Huber, A. S. Ferreira, S. D. Boyd, C. K. Luscombe, S. H. Tolbert and B. J. Schwartz, Crystallinity Effects in Sequentially Processed and Blend-Cast Bulk-Heterojunction Polymer/Fullerene Photovoltaics, *J. Phys. Chem. C*, 2014, **118**, 18424–18435, DOI: 10.1021/jp5054315.
- 160 X. Lin, J. Seok, S. Yoon, T. Kim, B. Kim and K. Kim, Morphological Investigation of P3HT/PCBM Heterojunction and Its Effects on the Performance of Bilayer Organic Solar Cells, *Synth. Met.*, 2014, **196**, 145–150, DOI: 10.1016/j.synthmet.2014.07.008.
- 161 Y. Syu, P. Huang, H. Li, C. Hsu, K. Chiu, C. Kim, M. Chen and Y. Chao, Enhanced Performance of Pseudo-Bilayer Organic Photovoltaic Devices via Small Molecule Doping, *J. Phys. Chem. C*, 2014, **118**, 9958–9965, DOI: 10.1021/jp502331x.
- 162 L. Xie, S. Yoon, Y. J. Cho and K. Kim, Effective Protection of Sequential Solution-Processed Polymer/Fullerene Bilayer Solar Cell against Charge Recombination and Degradation, *Org. Electron.*, 2015, **25**, 212–218, DOI: 10.1016/j.orgel.2015.06.039.
- 163 M. Casalegno, D. Kotowski, A. Bernardi, S. Luzzati, R. Po and G. Raos, The Effect of Donor Content on the Efficiency of P3HT:PCBM Bilayers: Optical and Photocurrent Spectral Data Analyses, *Phys. Chem. Chem. Phys.*, 2015, **17**, 2447–2456, DOI: 10.1039/c4cp03827d.
- 164 J. Lee, Y. Kyung, D. Yong, J. Jang, S. Cho, S. Son, J. Jeong and S. Heum, Enhanced Efficiency of Bilayer Polymer Solar Cells by the Solvent Treatment Method, *Synth. Met.*, 2015, **199**, 408–412, DOI: 10.1016/j.synthmet.2014.12.013.
- 165 C. Zhang, Y. Hu, A. Tang, Z. Deng and F. Teng, Investigating the Reduction in the Absorption Intensity of P3HT in Polymer/ Fullerene “Bilayers” Coated Using Orthogonal Solvents, *J. Appl. Polym. Sci.*, 2015, **117**, 1–5, DOI: 10.1002/app.41757.
- 166 Y. Jang, J. Seo, J. Seok, J. Lee and K. Kim, Roughening Conjugated Polymer Surface for Enhancing the Charge Collection Efficiency of Sequentially Deposited Polymer/ Fullerene Photovoltaics, *Polym. Eng. Sci.*, 2015, **7**, 1497–1509, DOI: 10.3390/polym7081466.
- 167 J. C. Aguirre, S. A. Hawks, A. S. Ferreira, P. Yee, S. Subramaniyan, S. A. Jenekhe, S. H. Tolbert and B. J. Schwartz, Sequential Processing for Organic Photovoltaics: Design Rules for Morphology Control by Tailored Semi-Orthogonal Solvent Blends, *Adv. Drug Delivery Rev.*, 2015, **95**(1402020), 1–11, DOI: 10.1002/aenm.201402020.
- 168 V. Vohra, B. Dörling, K. Higashimine and H. Murata, Investigating the Effect of Solvent Boiling Temperature on the Morphology of P3HT:PCBM Diffusive Bilayer Solar Cells, *Appl. Phys. Express*, 2016, **9**(012301), 1–4, DOI: 10.7567/APEX.9.012301.
- 169 Y. H. Huh, I.-G. Bae, H. G. Jeon and B. Park, Homogeneous PCBM Layers Fabricated by Horizontal-Dip Coating for Efficient Bilayer Heterojunction Organic Photovoltaic Cells, *Opt. Express*, 2016, **24**(22), 732–742, DOI: 10.1364/OE.24.0A1321.
- 170 A. Yi, S. Chae, S. Hong, H. H. Lee and H. J. Kim, Manipulating the Crystal Structure of a Conjugated Polymer for Efficient Sequentially Processed Organic Solar Cells, *Nanoscale*, 2018, **10**, 21052–21061, DOI: 10.1039/c8nr05407j.



- 171 M. T. Fontana, H. Kang, P. Y. Yee, Z. Fan, S. A. Hawks, L. T. Schelhas, S. Subramaniam, Y. Hwang, S. A. Jenekhe, S. H. Tolbert and B. J. Schwartz, Low-Vapor-Pressure Solvent Additives Function as Polymer Swelling Agents in Bulk Heterojunction Organic Photovoltaics, *J. Phys. Chem. C*, 2018, **122**, 16574–16588, DOI: 10.1021/acs.jpcc.8b04192.
- 172 S. Thakur, S. Rarotra, M. Bhattacharjee, S. Mitra, G. Natu, T. K. Mandal, A. K. Dasmahapatra and D. Bandyopadhyay, Self-Organized Large-Scale Integration of Mesoscale-Ordered Heterojunctions for Process-Intensified Photovoltaics, *Phys. Rev. Appl.*, 2018, **10**(064012), 1–15, DOI: 10.1103/PhysRevApplied.10.064012.
- 173 D. H. Wang, J. S. Moon, J. Seifert, J. Jo, J. H. Park, O. O. Park and A. J. Heeger, Sequential Processing: Control of Nanomorphology in Bulk Heterojunction Solar Cells, *Nano Lett.*, 2011, **11**, 3163–3168, DOI: 10.1021/nl202320r.
- 174 T. Kim, S. J. Yang, S. K. Kim, H. S. Choi and C. R. Park, Preparation of PCDTBT Nanofibers with a Diameter of 20 nm and Their Application to Air-Processed Organic Solar Cells †, *Nanoscale*, 2014, **6**, 2847–2854, DOI: 10.1039/c3nr05538h.
- 175 D. H. Kim, J. Mei, A. L. Ayzner, K. Schmidt, G. Giri, A. L. Appleton, F. Toney and Z. Bao, Sequentially Solution-Processed, Nanostructured Polymer Photovoltaics Using Selective Solvents †, *Energy Environ. Sci.*, 2014, **7**, 1103–1109, DOI: 10.1039/c3ee43541e.
- 176 J. Seok, T. J. Shin, S. Park, C. Cho, J. Y. Lee, D. Y. Ryu, M. H. Kim and K. Kim, Efficient Organic Photovoltaics Utilizing Nanoscale Heterojunctions in Sequentially Deposited Polymer/Fullerene Bilayer, *Sci. Rep.*, 2015, **5**(8373), 1–9, DOI: 10.1038/srep08373.
- 177 S. Ahn, W. Jang, J. Hyeok and D. Hwan, Enhanced Performance of Layer-Evolved Bulk-Heterojunction Solar Cells with Ag Nanoparticles by Sequential Deposition, *Org. Electron.*, 2015, **24**, 325–329, DOI: 10.1016/j.orgel.2015.05.008.
- 178 Y. Liu, F. Liu, H. Wang, D. Nordlund, Z. Sun, S. Ferdous and T. P. Russell, Sequential Deposition: Optimization of Solvent Swelling for High-Performance Polymer Solar Cells, *ACS Appl. Mater. Interfaces*, 2015, **7**, 653–661, DOI: 10.1021/am506868g.
- 179 J. J. Van Franeker, S. Kouijzer, X. Lou, M. Turbiez, M. M. Wienk and R. A. J. Janssen, Depositing Fullerenes in Swollen Polymer Layers via Sequential Processing of Organic Solar Cells, *Adv. Energy Mater.*, 2015, **5**(1500464), 1–10, DOI: 10.1002/aenm.201500464.
- 180 M. Kim, S. Park, D. Yeol and K. Kim, Improving Thermal Stability of Organic Photovoltaics via Constructing Interdiffused Bilayer of Polymer/Fullerene, *Polymer*, 2016, **103**, 132–139, DOI: 10.1016/j.polymer.2016.09.053.
- 181 C. Lang, J. Fan, Y. Zhang, F. Guo and L. Zhao, Utilizing Intermixing of Conjugated Polymer and Fullerene from Sequential Solution Processing for Efficient Polymer Solar Cells, *Org. Electron.*, 2016, **36**, 82–88, DOI: 10.1016/j.orgel.2016.05.036.
- 182 H. Hwang, H. Lee, S. Shafian, W. Lee, J. Seok, K. Y. Ryu, D. Y. Ryu and K. Kim, Thermally Stable Bulk Heterojunction Prepared by Sequential Deposition of Nanostructured Polymer and Fullerene, *Polymers*, 2017, **9**(456), 1–13, DOI: 10.3390/polym9090456.
- 183 Y. Choi, B. Hoon and H. Kim, Bicontinuous Network of Electron Donor-Acceptor Composites Achieved by Additive-Free Sequential Deposition for Efficient Polymer Solar Cells, *Curr. Appl. Phys.*, 2020, **20**, 760–764, DOI: 10.1016/j.cap.2020.03.011.
- 184 H. Li, Y.-F. Li and J. Wang, Optimizing Performance of Layer-by-Layer Processed Polymer Solar Cells, *Appl. Phys. Lett.*, 2012, **101**(033907), 1–4, DOI: 10.1063/1.4737877.
- 185 L. N. S. A. Thummalakunta, C. H. Yong, K. Ananthanarayanan and J. Luther, P3HT Based Solution-Processed Pseudo Bi-Layer Organic Solar Cell with Enhanced Performance, *Org. Electron.*, 2016, **13**, 2008–2016, DOI: 10.1016/j.orgel.2012.05.054.
- 186 J. H. Yim, S. Joe, D. C. Nguyen, S. Y. Ryu, N. Y. Ha, Y. H. Ahn, J. Park and S. Lee, True Nature of Active Layers in Organic Solar Cells Fabricated by Sequential Casting of Donor and Acceptor Layers, *Phys. Status Solidi RRL*, 2017, **11**(2), 1–4, DOI: 10.1002/pssr.201600415.
- 187 Y. J. Kim and C. E. Park, Well Defined Double Layers via Binary Solvent Mixtures for Highly Efficient Inverted All-Polymer Solar Cells, *Org. Electron.*, 2018, **52**, 301–308, DOI: 10.1016/j.orgel.2017.11.014.
- 188 J. Zhang, B. Kan, A. J. Pearson, A. J. Parnell, J. F. K. Cooper, X. Liu, P. J. Conaghan and R. H. Friend, Efficient Non-Fullerene Organic Solar Cells Employing Sequentially Deposited Donor-Acceptor Layers †, *J. Mater. Chem. A*, 2018, **6**, 18225–18233, DOI: 10.1039/c8ta06860g.
- 189 L. Ye, Y. Xiong, Z. Chen, Q. Zhang, Z. Fei, R. Henry, M. Heeney, B. T. O. Connor, W. You and H. Ade, Sequential Deposition of Organic Films with Eco-Compatible Solvents Improves Performance and Enables Over 12%-Efficiency Nonfullerene Solar Cells, *Adv. Mater.*, 2019, **31**(1808153), 1–9, DOI: 10.1002/adma.201808153.
- 190 J. Zhang, M. H. Futscher, V. Lami, F. U. Kosasih, C. Cho, Q. Gu, A. Sadhanala, A. J. Pearson, B. Kan, G. Divitini, X. Wan, D. Credgington, N. C. Greenham, Y. Chen, C. Ducati, B. Ehrler, Y. Vaynzof, R. H. Friend and A. A. Bakulin, Sequentially Deposited versus Conventional Nonfullerene Organic Solar Cells: Interfacial Trap States, Vertical Stratification, and Exciton Dissociation, *Adv. Energy Mater.*, 2019, **9**(1902145), 1–9, DOI: 10.1002/aenm.201902145.
- 191 V. S. Gevaerts, L. J. A. Koster, M. M. Wienk and A. J. Janssen, Discriminating between Bilayer and Bulk Heterojunction Polymer: Fullerene Solar Cells Using the External Quantum Efficiency, *ACS Appl. Mater. Interfaces*, 2011, **3**, 3252–3255, DOI: 10.1021/am200755m.
- 192 N. D. Treat, M. A. Brady, G. Smith, M. F. Toney, E. J. Kramer, C. J. Hawker and M. L. Chabinye, Interdiffusion of PCBM and P3HT Reveals Miscibility in a Photovoltaically Active Blend, *Adv. Energy Mater.*, 2011, **1**, 82–89, DOI: 10.1002/aenm.201000023.
- 193 D. Môn, A. M. Higgins and D. James, Mixing in PCBM/P3HT Bilayers, Using in Situ and Ex Situ Neutron Reflectivity, *J. Mater. Res.*, 2017, **32**(10), 1946–1956, DOI: 10.1557/jmr.2017.59.



- 194 A. M. Nardes, A. L. Ayzner, S. R. Hammond, A. J. Ferguson, B. J. Schwartz and N. Kopidakis, Photoinduced Charge Carrier Generation and Decay in Sequentially Deposited Polymer/Fullerene Layers: Bulk Heterojunction vs Planar Interface, *J. Phys. Chem. C*, 2012, **116**, 7293–7305, DOI: 10.1021/jp212390p.
- 195 F. Nüesch, G. Tornare, L. Zuppiroli, F. Meng, K. Chen and H. Tian, Interface Modification to Optimize Charge Separation in Cyanine Heterojunction Photovoltaic Devices, *Sol. Energy Mater. Sol. Cells*, 2005, **87**, 817–824, DOI: 10.1016/j.solmat.2004.07.054.
- 196 X. Jiang, J. Dai, H. Wang and D. Yan, The Effect of Annealing Treatment on Performance of Interdiffused Organic Photovoltaic Devices, *Thin Solid Films*, 2008, **516**, 6487–6491, DOI: 10.1016/j.tsf.2008.02.026.
- 197 A. Geiser, B. Fan, H. Benmansour, F. Castro, J. Heier, B. Keller, K. Emanuel, F. Nu and R. Hany, Poly(3-Hexylthiophene)/C60 Heterojunction Solar Cells: Implication of Morphology on Performance and Ambipolar Charge Collection, *Sol. Energy Mater. Sol. Cells*, 2008, **92**, 464–473, DOI: 10.1016/j.solmat.2007.11.001.
- 198 B. Fan, F. A. De Castro, B. T. Chu, J. Heier, D. Opris, R. Hany and F. Nüesch, Improved Performance of Cyanine Solar Cells with Polyaniline Anodes, *J. Mater. Chem.*, 2010, **20**, 2952–2955, DOI: 10.1039/b925289d.
- 199 B. Fan, F. A. De Castro, J. Heier, R. Hany and F. Nüesch, High Performing Doped Cyanine Bilayer Solar Cell, *Org. Electron.*, 2010, **11**, 583–588, DOI: 10.1016/j.orgel.2009.12.017.
- 200 G. Wei, X. Xiao, S. Wang, J. D. Zimmerman, K. Sun, V. V. Diev, M. E. Thompson and S. R. Forrest, Arylamine-Based Squaraine Donors for Use in Organic Solar Cells, *Nano Lett.*, 2011, **11**, 4261–4264, DOI: 10.1021/nl2022515.
- 201 M. Lenes and H. J. Bolink, Ionic Space-Charge Effects in Solid State Organic Photovoltaics, *ACS Appl. Mater. Interfaces*, 2010, **2**(12), 3664–3668, DOI: 10.1021/am1008216.
- 202 G. Wicht, S. Bücheler, M. Dietrich, T. Jäger, F. Nüesch, T. Offermans, J. Tisserant, L. Wang, H. Zhang and R. Hany, Stability of Bilayer Trimethine Cyanine Dye/Fullerene Organic Solar Cells, *Sol. Energy Mater. Sol. Cells*, 2013, **117**, 585–591, DOI: 10.1016/j.solmat.2013.07.008.
- 203 E. Berner, T. Jäger, T. Lanz, F. Nüesch, J. Tisserant, G. Wicht, H. Zhang and R. Hany, Influence of Crystalline Titanium Oxide Layer Smoothness on the Performance of Inverted Organic Bilayer Solar Cells, *Appl. Phys. Lett.*, 2013, **183903**, 98–102, DOI: 10.1063/1.4804599.
- 204 S. Jenatsch, R. Hany, A. C. Véron, M. Neukom, S. Züfle, A. Borgschulte, B. Ruhstaller and F. Nüesch, Influence of Molybdenum Oxide Interface Solvent Sensitivity on Charge Trapping in Bilayer Cyanine Solar Cells, *J. Phys. Chem. C*, 2014, **118**, 17036–17045, DOI: 10.1021/jp5005314.
- 205 F. Zabihi, Q. Chen, Y. Xie and M. Eslamian, Fabrication of Efficient Graphene-Doped Polymer/Fullerene Bilayer Organic Solar Cells in Air Using Spin Coating Followed by Ultrasonic Vibration Post Treatment, *Superlattices Microstruct.*, 2016, **100**, 1177–1192, DOI: 10.1016/j.spmi.2016.10.087.
- 206 J. Huang, K. Li, D. Kekuda, H. H. Padhy, H. Lin, K.-C. Ho and C.-W. Chu, Efficient Bilayer Polymer Solar Cells Possessing Planar Mixed-Heterojunction Structures †, *J. Mater. Chem.*, 2010, **20**, 3295–3300, DOI: 10.1039/b924147g.
- 207 D. Kekuda, H. Lin, M. Chyi, J. Huang, K. Ho and C. Chu, The Effect of Solvent Induced Crystallinity of Polymer Layer on Poly(3-Hexylthiophene)/C70 Bilayer Solar Cells, *Sol. Energy Mater. Sol. Cells*, 2011, **95**, 419–422, DOI: 10.1016/j.solmat.2010.05.055.
- 208 D. S. Josey, J. S. Castrucci, J. D. Dang and B. H. Lessard, Evaluating Thiophene Electron-Donor Layers for the Rapid Assessment of Boron Subphthalocyanines as Electron Acceptors in Organic Photovoltaics: Solution or Vacuum Deposition?, *ChemPhysChem*, 2015, **16**, 1245–1250, DOI: 10.1002/cphc.201402751.
- 209 L. Lucera, P. Kubis, F. W. Fecher, C. Bronnbauer, M. Turbiez, K. Forberich, T. Ameri, H. Egelhaaf and C. J. Brabec, Guidelines for Closing the Efficiency Gap between Hero Solar Cells and Roll-To-Roll Printed Modules, *Energy Technol.*, 2015, **3**, 373–384, DOI: 10.1002/ente.201402192.
- 210 S. Hong, J. Lee, H. Kang and K. Lee, Slot-Die Coating Parameters of the Low-Viscosity Bulk-Heterojunction Materials Used for Polymer Solar Cells, *Sol. Energy Mater. Sol. Cells*, 2013, **112**, 27–35, DOI: 10.1016/j.solmat.2013.01.006.
- 211 D. Vak, K. Hwang, A. Faulks, Y. Jung, N. Clark, D. Kim, G. J. Wilson and S. E. Watkins, 3D Printer Based Slot-Die Coater as a Lab-to-Fab Translation Tool for Solution-Processed Solar Cells, *Adv. Energy Mater.*, 2015, **5**(1401539), 1–8, DOI: 10.1002/aenm.201401539.
- 212 S. Hong, H. Kang, G. Kim, S. Lee, S. Kim, J. Lee, J. Lee, M. Yi, J. Kim, H. Back, J. Kim and K. Lee, A Series Connection Architecture for Large-Area Organic Photovoltaic Modules with 7.5% Module Efficiency, *Nat. Commun.*, 2016, **7**(10279), 1–6, DOI: 10.1038/ncomms10279.
- 213 S. Song, K. T. Lee, C. W. Koh, H. Shin, M. Gao, H. Y. Woo, D. Vak and J. Y. Kim, Hot Slot Die Coating for Additive-Free Fabrication of High Performance Roll-to-Roll Processed Polymer Solar Cells, *Energy Environ. Sci.*, 2018, **11**, 3248–3255, DOI: 10.1039/c8ee02221f.
- 214 Q. Wu, J. Guo, R. Sun, J. Guo, S. Jia, Y. Li, J. Wang and J. Min, Slot-Die Printed Non-Fullerene Organic Solar Cells with the Highest Efficiency of 12.9% for Low-Cost PV-Driven Water Splitting, *Nano Energy*, 2019, **61**, 559–566, DOI: 10.1016/j.nanoen.2019.04.091.
- 215 G. Ji, W. Zhao, J. Wei, L. Yan, Y. Han, Q. Luo, S. Yang, J. Hou and C.-Q. Ma, 12.88% Efficiency in Doctor-Blade Coated Organic Solar Cells through Optimizing the Surface Morphology of a ZnO Cathode Buffer Layer†, *J. Mater. Chem. A*, 2019, **7**, 212–220, DOI: 10.1039/c8ta08873j.
- 216 Q. Kang, L. Ye, B. Xu, C. An, S. J. Stuard, S. Zhang, H. Yao, H. Ade and J. Hou, A Printable Organic Cathode Interlayer Enables over 13% Efficiency for 1-Cm<sup>2</sup> Organic Solar Cells, *Joule*, 2019, **3**, 227–239, DOI: 10.1016/j.joule.2018.10.024.
- 217 L. Ye, Y. Xiong, Q. Zhang, S. Li, C. Wang, Z. Jiang, J. Hou, W. You and H. Ade, Surpassing 10% Efficiency Benchmark for Nonfullerene Organic Solar Cells by Scalable Coating in Air from Single Nonhalogenated Solvent, *Adv. Mater.*, 2018, **30**(1705485), 1–9, DOI: 10.1002/adma.201705485.



- 218 W. Zhao, S. Zhang, Y. Zhang, S. Li, X. Liu, C. He, Z. Zheng and J. Hou, Environmentally Friendly Solvent-Processed Organic Solar Cells That Are Highly Efficient and Adaptable for the Blade-Coating Method, *Adv. Mater.*, 2018, **30**(1704837), 1–7, DOI: 10.1002/adma.201704837.
- 219 Q. Kang, Q. Liao, Y. Xu, L. Xu, Y. Zu, S. Li, B. Xu and J. Hou, P-Doped Conducting Polyelectrolyte as an Anode Interlayer Enables High Efficiency for 1 Cm<sup>2</sup> Printed Organic Solar Cells, *ACS Appl. Mater. Interfaces*, 2019, **11**, 20205–20213, DOI: 10.1021/acsami.9b04211.
- 220 Q. Kang, B. Yang, Y. Xu, B. Xu and J. Hou, Printable MoO<sub>x</sub> Anode Interlayers for Organic Solar Cells, *Adv. Mater.*, 2018, **30**(1801718), 1–7, DOI: 10.1002/adma.201801718.
- 221 J. Chang, H. Wang, W. Lin, K. Chiang, K. Chen, W. Huang, Z. Huang, H. Meng, R. Ho and H. Lin, Efficient Inverted Quasi-Bilayer Organic Solar Cells Fabricated by Using Non-Halogenated Solvent, *J. Mater. Chem. A*, 2014, **2**, 13398–13406, DOI: 10.1039/c4ta02453b.
- 222 R. Sun, J. Guo, Q. Wu, Z. Zhang, W. Yang, J. Guo, M. Shi, Y. Zhang, S. Kahmann, L. Ye, X. Jiao, M. A. Loi, Q. Shen, H. Ade, T. Weihua, C. J. Brabec and J. Min, A Multi-Objective Optimization-Based Layer-by-Layer Blade-Coating Approach for Organic Solar Cells: Rational Control of Vertical Stratification for High Performance, *Energy Environ. Sci.*, 2019, **12**, 3118–3132, DOI: 10.1039/c9ee02295c.

